RUSSIAN ACADEMY OF SCIENCES

NATIONAL GEOPHYSICAL COMMITTEE

РОССИЙСКАЯ АКАДЕМИЯ НАУК

НАЦИОНАЛЬНЫЙ ГЕОФИЗИЧЕСКИЙ КОМИТЕТ

NATIONAL REPORT

for the

International Association for the
Physical Sciences of the Oceans

of the

International Union of Geodesy and Geophysics

2011–2014

НАЦИОНАЛЬНЫЙ ОТЧЕТ

Международной ассоциации
физических наук об океане
Международного
геодезического и геофизического союза

2011–2014

Москва 2015 Moscow

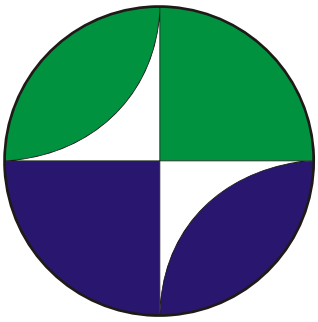

Presented to the XXVI General Assembly
of the
International Union of Geodesy and Geophysics

К XXVI Генеральной ассамблее
Международного геодезического и геофизического союза

RUSSIAN ACADEMY OF SCIENCES

National Geophysical Committee

NATIONAL REPORT

for the

International Association for the
Physical Sciences of the Oceans

of the

International Union of Geodesy and Geophysics

2011–2014

Presented to the XXVI General Assembly

of the

IUGG

2015

Moscow

This report presents the activity of the Russian oceanographers for the period of 2011–2015. The short reports are presented by the authors of researches.

The following institutes participated in the preparation of this report:
Shirshov Institute of Oceanology, RAS (Moscow) and its departments in St. Petersburg and Kaliningrad;
Il'ichev Pacific Institute of Oceanology, FEB RAS (Vladivostok);
Andreev Acoustic Institute (Moscow);
Institute of Applied Physics, RAS (Nizhny Novgorod);
Lavrentiev Institute of Hydrodynamics, SB RAS (Novosibirsk).

The report was prepared by the following scientists:
S. Badulin, M. Budyansky, V. Byshev, T. Demidova, I. Didenkulova, E. Dmitriyeva, V. Dubina, A. Falina, P. Fayman, B. Filyushkin, T. Kleshcheva, M. Koshlyakov, A. Kostianoy, A. Kubryakov, E. Kulikov, N. Makarenko, I. Mashkina, E. Morozov, V. Navrotsky, V. Neiman, V. Novotryasov, V. Paka, E. Pelinovsky, M. Permyakov, V. Ponomarev, S. Prants, A. Rabinovich, A. Rodionov, A. Sarafanov, N. Savelyeva, A. Serebryany, A. Sergeeva, I. Serykh, S. Shkorba, V. Shrira, A. Slunyaev, M. Sokolovskiy, A. Sokov, D. Sonechkin, S. Stanichny, D. Stepanov, R. Tarakanov, T. Talipova, O. Trusenkova, M. Uleysky, A. Zatsepin, P. Zavialov, V. Zhurbas.

В данном отчете представлены результаты российских океанографов в 2011–2015 гг. Авторами исследований были подготовлены краткие обзоры.

В подготовке данного отчета принимали участие представители следующих организаций:
Институт океанологии им. П.П. Ширшова РАН (Москва) и его филиалы Санкт-Петербурге и Калининграде;
Тихоокеанский океанологический институт им. В.И. Ильичева ДВО РАН (Владивосток);
Акустический институт им. Н.Н. Андреева (Москва);
Институт прикладной физики РАН (Нижний Новгород);
Институт гидродинамики им. М.А. Лаврентьева СО РАН (Новосибирск).

В подготовке данного отчета принимали участие:
С. Бадулин, М. Будянский, В. Бышев, Т. Демидова, И. Диденкулова, Е. Дмитриева, В. Дубина, В. Журбас., П. Завьялов, А. Зацепин, Т. Клещева, М. Кошляков, А. Костяной, А. Кубряков, Е. Куликов, Н. Макаренко, И. Машкина, Е. Морозов, В. Навротский, В. Нейман, В. Новотрясов, В. Пака, Е. Пелиновский, М. Пермяков, В. Пономарев, С. Пранц, А. Рабинович, А. Родионов, А. Сарафанов, Н Савельева, А. Серебряный, А. Сергеева, И. Серых, С. Шкобра, В. Шрира, А. Слюняев, М. Соколовский, А. Соков, Д. Сонечкин, С. Станичный, Д. Степанов, Р. Тараканов, Т. Талипова, О. Трусенкова, М. Улецкий, П. Файман, А. Фалина, Б. Филюшкин.

DOI: **10.2205/2015IUGG-RU-IAPSO**

Citation: Morozov E.G. Ed. (2015), National Report for the IAPSO of the IUGG 2011–2014, *Geoinf. Res. Papers*, 3, BS3009, GCRAS Publ., Moscow, 59 pp. doi: 10.2205/2015IUGG-RU-IAPSO

Executive Summary

The main scientific results obtained by the Russian oceanographers are briefly presented. The transports in the entire water column of the open ocean from the eastern coast of Greenland to Northern Europe were estimated. The flows of Antarctic Bottom Water through the Kane Gap (9° N) in the Atlantic was investigated as well as the flow of AABW into the Romanche Fracture Zone. Antarctic Bottom Water flows into the Romanche FZ through a narrow gap in the western part of the fracture. The mean horizontal velocities of the flow near the bottom are 0.40 m/s. An abyssal cyclonic eddy with a horizontal size of 100 km that does not penetrate above 1500 m was found in the Yagan Basin in the region of the Drake Passage. We found that the geographical location of abyssal eddies coincided with the similar vortexes of the Antarctic Circumpolar Current in the upper ocean. Meandering of the ACC jet in the thermocline leads to the compression of tension of the vertical water columns in the abyssal depths; therefore owing to the law of potential vorticity conservation it forms the eddies of the same sign as in the thermocline.

Mean global sea-level pressure fields corresponding to the 23 El-Niño and 25 La-Niña events observed in 1920-2012 were considered. The regions of the Earth were revealed, in which systematic differences exist between the El-Niño and La-Niña events. These are the polar regions of Canada and Pacific, Indonesia, and the near equatorial Atlantic and African regions.

Dynamics of intrathermocline lenses in the ocean was analyzed The analysis of historical observations has showed that approximately 100 lenses can exist simultaneously in this part of the ocean.

Researches were conducted in the northern seas of Russia and other marginal seas around the country. A numerical model was developed to calculate the ice cover in the Barents Sea throughout the year. The maximum ice cover was found in 2003 and the minimum in 2002. Seasonal and interannual variability of air temperature, atmospheric precipitation, wind speed, sea level, sea surface temperature, ice cover, salinity, and river runoff duirng the period from 1979 to 2011 and water areas of all the Russian seas were studied.

Long-term field and satellite observations in the shelf regions adjacent to small Russian rivers of the Caucasian coast were analyzed. Clearly manifested river plumes in the surface layer 1-4 m thick were found. The mesoscale circulation in the Black sea experienced strong changes after 2002-2003. It was revealed that the variability of the mesoscale eddy energy is in the opposite phase to the mean kinetic energy of the Black Sea circulation because the weakening of the Black Sea Rim Current leads to its instability and the formation of the mesoscale anticyclones, while the strengthening of the Rim current suppresses the instability and mesoscale eddy formation.

Measurements and modeling were carried out to study the flow in the Slupsk Furrow, a channel-like topographic constriction in the southern Baltic Sea between the Bornholm Basin and the Eastern Gotland/Gdansk basins, which is the only pathway for salty water from the North Sea to enter the deep basins of the Baltic Sea and ventilate them laterally.

Several statistically significant and physically meaningful variability patterns of sea level and eddy kinetic energy in the Japan Sea are detected by means of multivariate analysis of satellite altimetry data. Winter anomalies of the oceanographic characteristics in the Okhotsk and Japan Seas were detected on the interannual, decadal and interdecadal time scales and their linkages with surface heat flux in the North Pacific Ocean were revealed. Using high resolution satellite imagery and simulations with the eddy resolving oceanic model, dynamic structures on the shelf, over continental slope and in deep basin of the Northwestern Japan Sea were studied. Intra-seasonal and seasonal variability, including formation, movement, interaction, and

decay of mesoscale and sub-mesoscale anticyclonic and cyclonic eddies, were revealed.

Relationship between sea surface temperature and surface wind speed and direction were revealed in the Okhotsk Sea, and after the propagation of typhoons.

A model of surface wave steepness was developed to estimate the steepness and of waves and their period from satellite altimetry measurements.

High-quality data were used to examine the physics of tsunami generation and propagation, in particular the tsunami energy decay. Numerical simulations of intense irregular waves were performed for conditions of laboratory experiments and for given sea states to obtain the true statistics of rogue waves taking into account strongly nonlinear effects. An asymptotic modal approach is developed for waves trapped by an opposing jet current in linear and nonlinear settings.

Contents

Stochastic modelling of rogue waves
A. Slunyaev, A. Sergeeva, E. Pelinovsky, I. Didenkulova

Reconstruction of in-situ events of rogue waves
A. Slunyaev, A. Sergeeva, E. Pelinovsky, T. Talipova

Simulations of long-living coherent wave patterns as
prototypes of rogue waves
A. Slunyaev, E. Pelinovsky, A. Sergeeva

Rogue wave generation on opposing jet currents
due to nonlinear self-modulation
V. Shrira, A. Slunyaev

Spectral model of nonlinear internal waves in the coastal ocean
V.V. Novotryasov, D.V. Stepanov

Effects of internal waves in a shoaling thermocline
V. Navrotsky

Dissipation-derived estimates of entrainment in the Denmark Strait overflow plume
V. Paka

Observations of mode 2 internal waves on shelf of the Black Sea
A. Serebryany

References:

Circulation in the North Atlantic

A. Sarafanov, A. Falina, A. Sokov

We estimated the transports in the entire water column of the open ocean from the eastern coast of Greenland to Northern Europe. The main mechanism of the transformation of warm surface waters transported to the north by the North Atlantic Current to the cold dense subarctic waters is gradual cooling in the course of their propagation to the north. Previously it was considered that the main role in the formation of the lower circulation link in the North Atlantic belongs to the winter convection in the Labrador Sea. Our data of observations in the last years over the section along 59°30' N and in the Strait of Denmark and Faroe-Shetland Strait made us reconsider this concept.

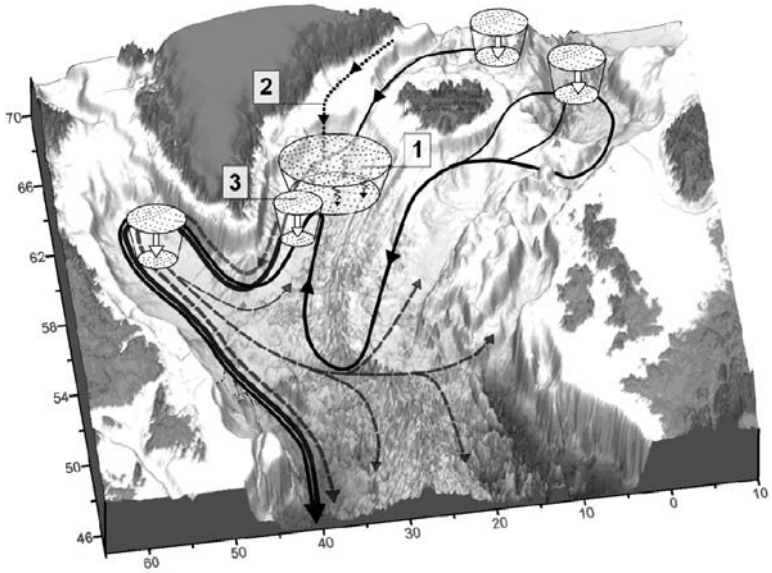

Modern changes in the concept of 3D circulation in the subarctic Atlantic based on the recent measurements. The solid arrows show the pathways of dense water formed in the Arctic region. Dashed arrows show the pathways of the waters formed in the Labrador Sea. Cylinders with arrows show the regions of deep convection. Numerals show the mechanisms whose contribution to the formation of the lower link of circulation has not been taken into account until recently: (1) transformation of surface waters in the Northeast Atlantic (convection to ~500 m); (2) cascading of the shelf waters in the northern part of the Irminger Sea, and (3) deep convection in the Irminger Sea (up to > 1000 m).

Abyssal flows

E. Morozov, R. Tarakanov, N. Makarenko, T. Demidova

A scheme of Antarctic Bottom Water flow in the Atlantic is shown in the figure below.

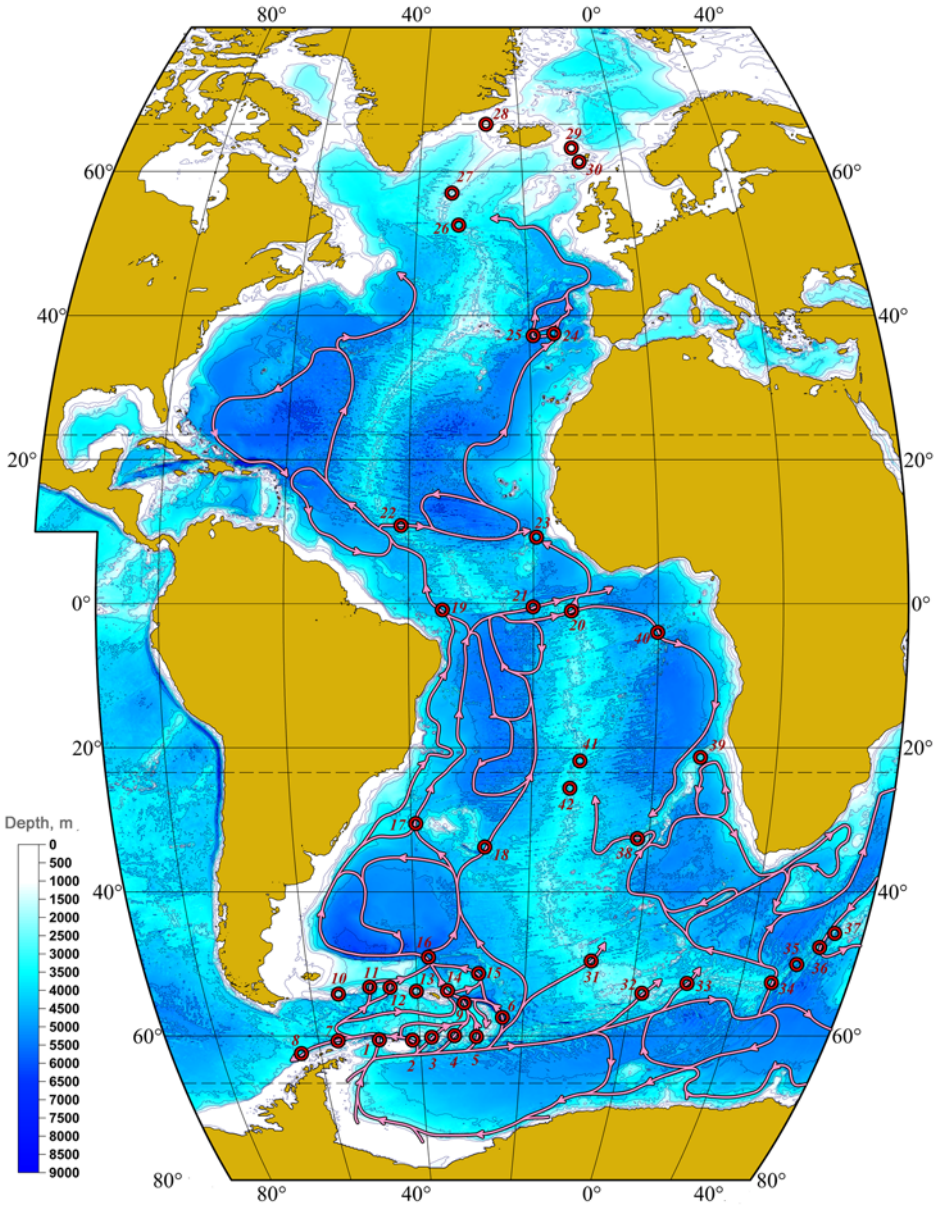

Kane Gap

The flow of Antarctic Bottom Water through the Kane Gap (9° N) in the Atlantic was investigated. The CTD/LADCP measurements in the Kane Gap were conducted in 2009-2012. A year-long record of currents on a mooring using three AquaDopp current-meters was obtained. We found an alternating regime of flow, which changes direction several times during a year. The seasonal signal dominates. The maximum daily average southerly velocities reach 0.20 m s^{-1}, while the highest north-northwesterly velocity was as high as 0.15 m s^{-1}. The transport of Antarctic Bottom Water (Θ < 1.9°C) based on the mooring and LADCP data varies approximately within ±0.35 Sv in the northern and southern directions. The annual mean AABW transport through the Kane Gap is almost zero.

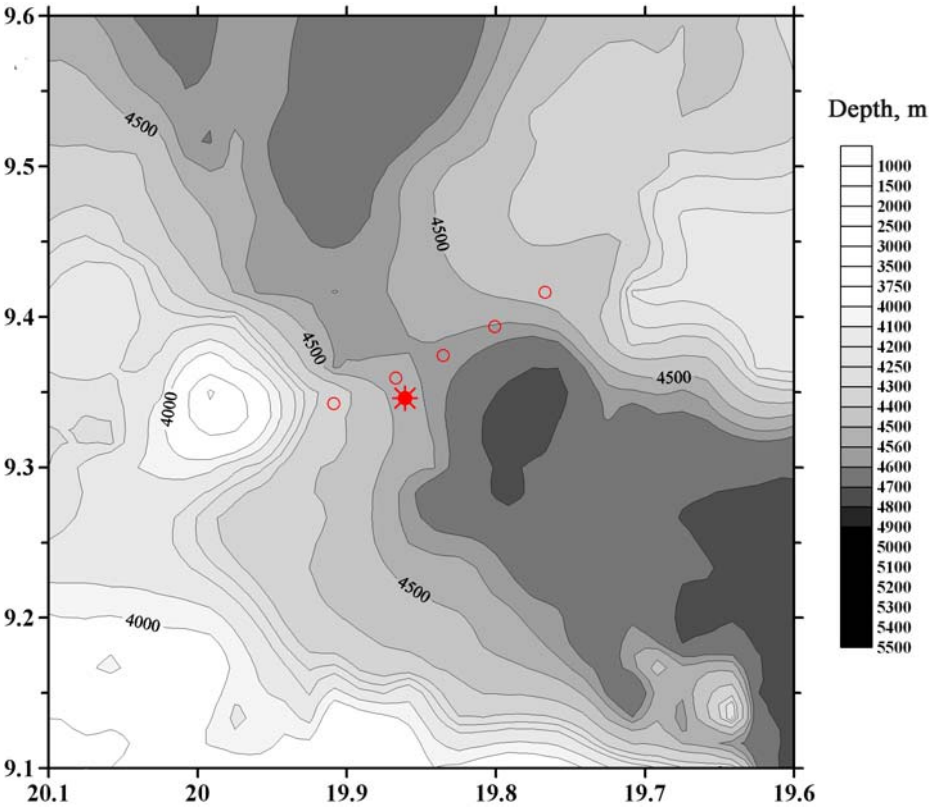

Bottom topography in the Kane Gap, locations of CTD/LADCP stations and location of the mooring (asterisk)

Romanche Fracture Zone

Antarctic Bottom Water flows into the Romanche FZ through a narrow gap in the western part of the fracture. A deep-water cataract exists in this gar approximately at 01°05' S, 22°27' W. Measurements with CTD and LADCP in this passage were repeated four times in 2011-2014. A mooring was deployed in the cataract for six months. The mean horizontal velocities of the flow near the bottom are 0.40 m/s. The slope of the flow in the cataract is 1/10. The transport of bottom water below the level of potential temperature 1.70°C based on the LADCP measurements is 0.25 Sv, which is approximately 40% of the known transport estimates through the fracture in its middle part. The cataract is a cascade of the flow initially over two sills with depths of 4570 and 4430 m, and then they merge in a flow over a sill of 4870 m deep. Extremely strong mixing is found in the region of the cataract.

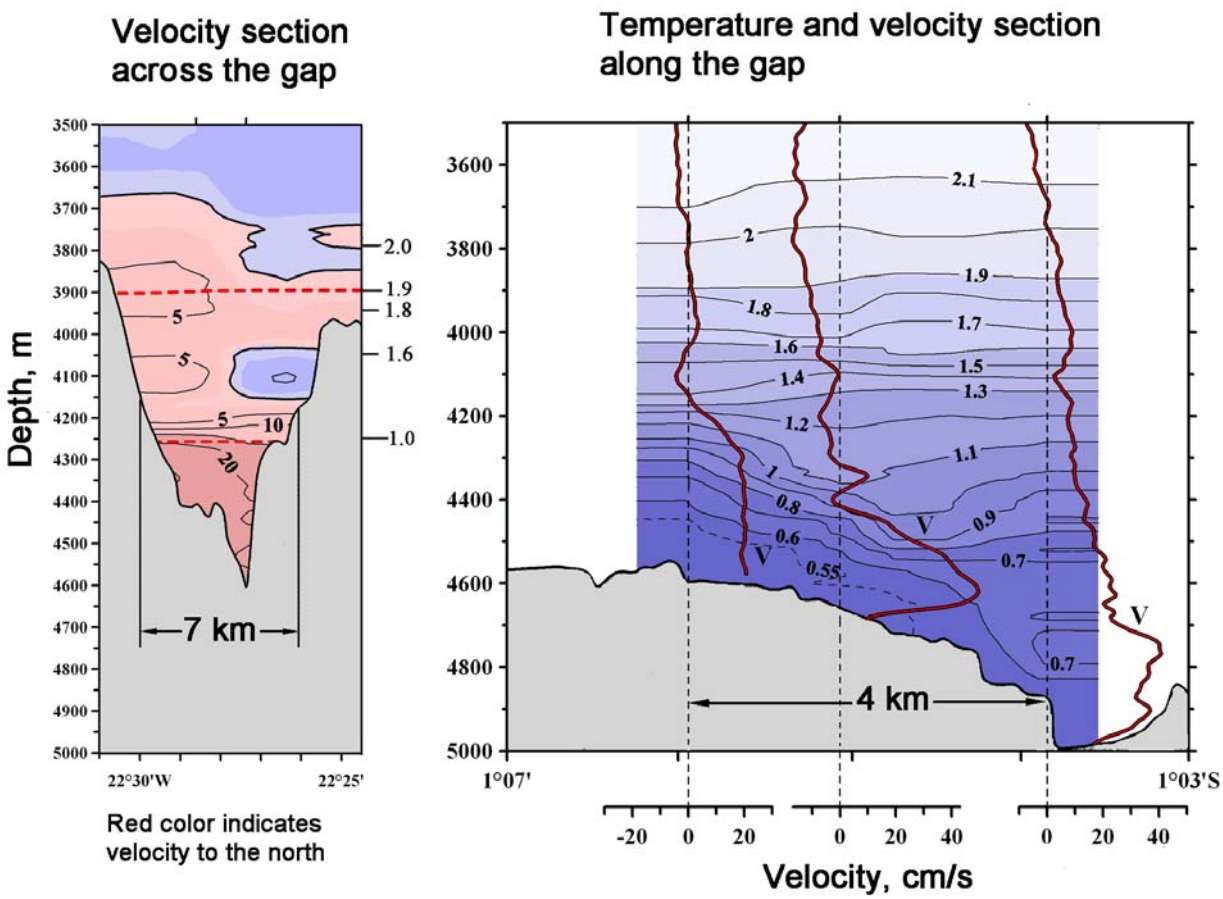

Temperature and velocity sections across and along the gap, through which AABW flows into the Romanche FZ

Abyssal eddies in the Drake Passage

M. Koshlyakov, R. Tarakanov

An abyssal cyclonic eddy with a horizontal size of 100 km that does not penetrate above 1500 m was found in the Yagan Basin. Similar eddies were later again found not only in the Yagan but also in the Phoenix Basin. Five abyssal eddies are seen in the figure: three anticyclones and two cyclones. The upper boundaries of the eddies were located at 1500-2500 m. The characteristic velocities ranged from 10 to 25 cm/s. We found that the geographical location of abyssal eddies coincided with the similar vortexes of the Antarctic Circumpolar Current in the upper ocean. This makes us think that the formation mechanism of abyssal eddies in the Drake Passage is similar to the mechanism of formation of the atmospheric eddies at the Earth's surface. Meandering of the ACC jet in the thermocline leads to the compression of tension of the vertical water columns in the abyssal depths; therefore owing to the law of potential vorticity conservation it forms the eddies of the same sign as in the thermocline.

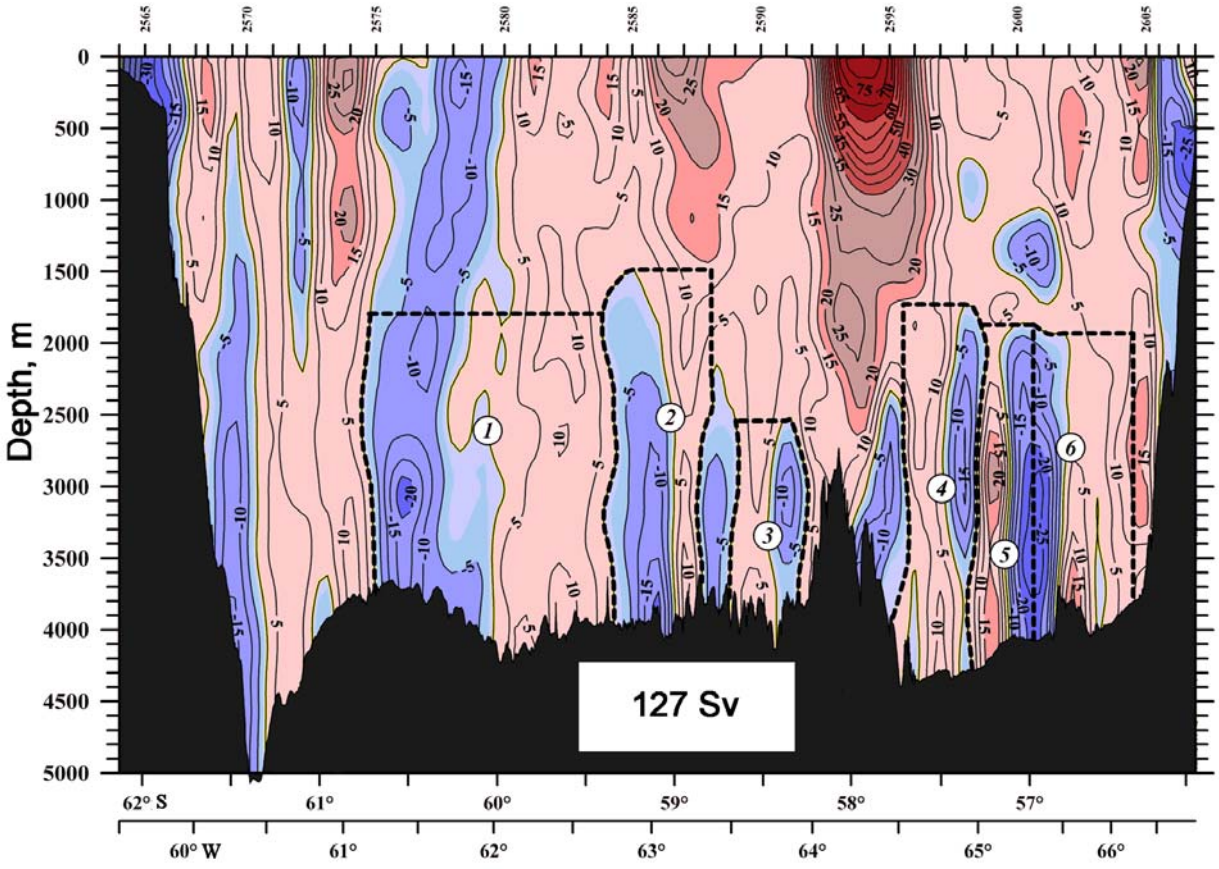

Normal velocity component to the section across the Drake Passage measured in November-December, 2011 (cm/s) based on the LADCP data. Red color shows the northeastern velocities, blue color indicates southwestern velocities. Dashed lines and numerals in circles show the boundaries and numbers of individual cyclonic and anticyclonic eddies. The total transport through the strait is 127 Sv.

The ENSO is a non-chaotic subsystem of the global climatic system

D. Sonechkin, V. Neiman, I. Serykh, V. Byshev

We consider the monthly mean global sea-level pressure fields corresponding to the 23 El-Niño and 25 La-Niña events observed in 1920-2012. The regions of the Earth were revealed, in which systematic differences exist between the El-Niño and La-Niña events. We found such regions almost everywhere on the Earth as well as it has been done in many previous investigations. The statistical significance of each area was estimated for the first time using the *t-Student* test. The results of these tests are shown in Fig. 1 by red (positive differences) and blue colors (negative differences). The areas outlined by *t-Student* contour ± 2 are significant at a level of 0.05. The examples are symmetric with respect to the equator; the blue colored areas are located in the Atlantic and in the polar regions of Canada and Pacific. However, there are much more significant areas, e.g. Indonesia (t=+12), the classic El-Niño area (t=-8), and the near equatorial Atlantic and African regions (t=+6). This structure itself and the cross-correlations computed between all pairs of the significant areas provide evidence that a strong coupling exists between the processes in all indicated regions. However, unlike the generally accepted opinion, the ENSO is not a cause of the processes far from the equatorial Pacific, but instead it is affected by all of these processes. Figuratively speaking, El-Niño is a “rogue wave” in the global dynamics of the climatic system.

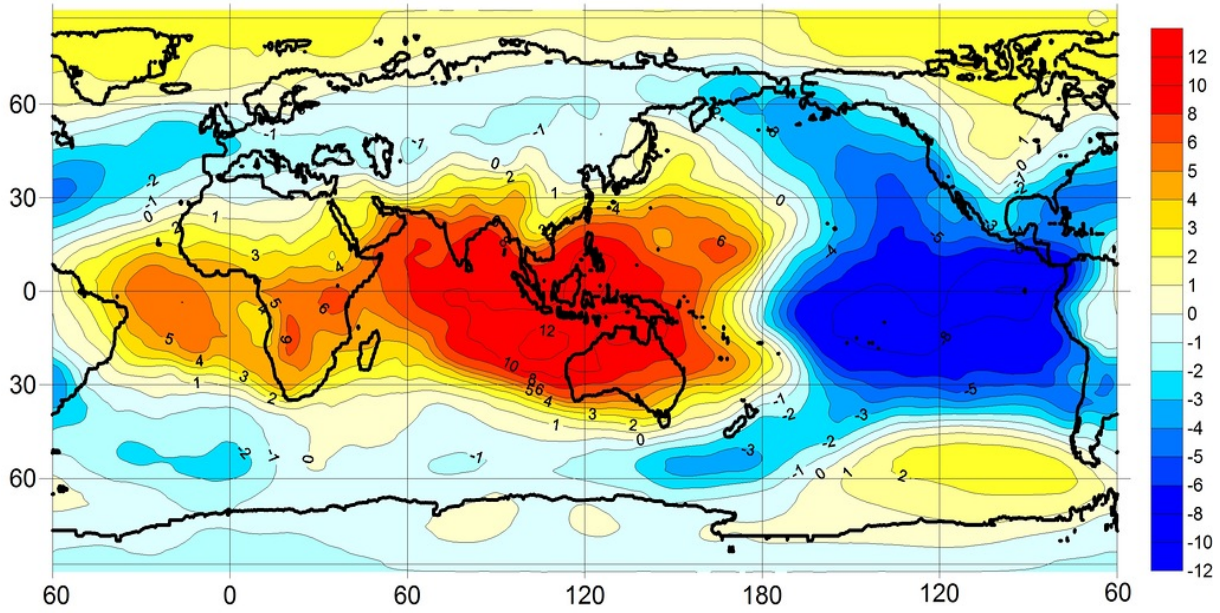

Fig. 1 Global map of the statistical significance (*t-Student* test) of the mean differences between the sea-level atmospheric pressure corresponding to the 23 El-Niño and 25 La-Niño events observed in the period 1920 – 2012. Red (blue) colored domains are related to positive (negative) differences. The values $t=\pm 2$ and greater outline the regions of significant differences at a level of 0.05 or greater.

The ENSO is also affected by many external forces. In addition to the annual Sun-induced periodic heating, which is a well-known driver of the ENSO, the so-called Chandler wobble in the Earth’s pole motion (of 1.2-year long period) is likely to be the most important because the main peaks in the power spectrum of the ENSO are localized near the periods equal to doubled (2Ch=2.4y), trebled (3Ch=3.6y), and quadrupled (4Ch=4.8y) Chandlerian periods. It can be seen in Fig. 2 where Nino-3+4 index spectra are shown, which were computed for the time series of each month of the year taken separately in order to damp harmonics of the annual period, thus

emphasizing the ENSO-variations of longer scales. Perhaps, some higher degree sub-harmonics of the Chandler wobble exist in the spectrum, but they can not be reliably recognized because of the finite lengths of the observational records and their noisiness.

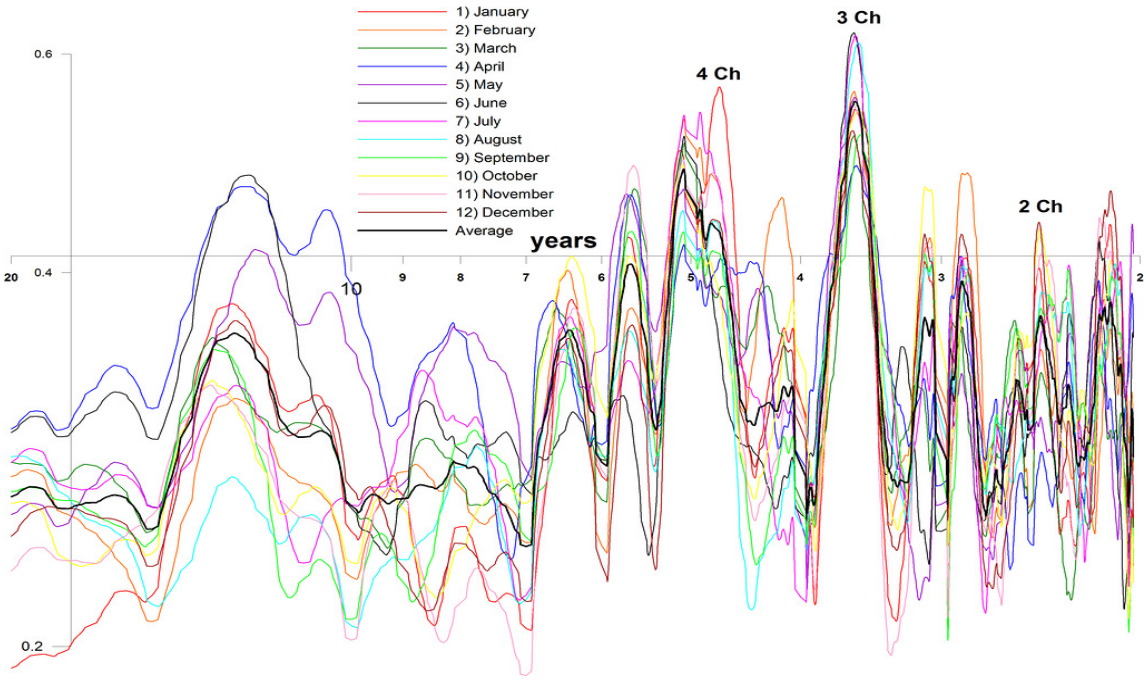

Fig. 2 Power spectrum of a Nino 3+4 index computed for the time series of each month of the year taken separately over the 1920 – 2012 time interval (shown on the logarithmic coordinate scales). The averaged spectrum is shown by the heavy black line. The peaks of the doubled, trebled, and quadrupled Chandlerian periods are marked.

The mathematical theory of the nonlinear dynamical systems indicates that the interrelation between the magnitudes of the power spectrum peaks and their serial numbers is indicative to decide whether the variations in the time series of interest are chaotic or non-chaotic. In the first case, this interrelation has to look like a straight line on the logarithmic coordinate scales. But, in the second case, it has to look like a polynomial of the *n*-th degree where the value of *n* is equal to the number of the external forces, which essentially affect the time series. Figure 3 shows such an interrelation computed on the basis of the ENSO spectrum shown in Fig. 2. One can see that a quadratic polynomial approximates the interrelation quite well. Therefore, two external forces (the annual heating and the Chandler wobble) seem to be the essential drivers.

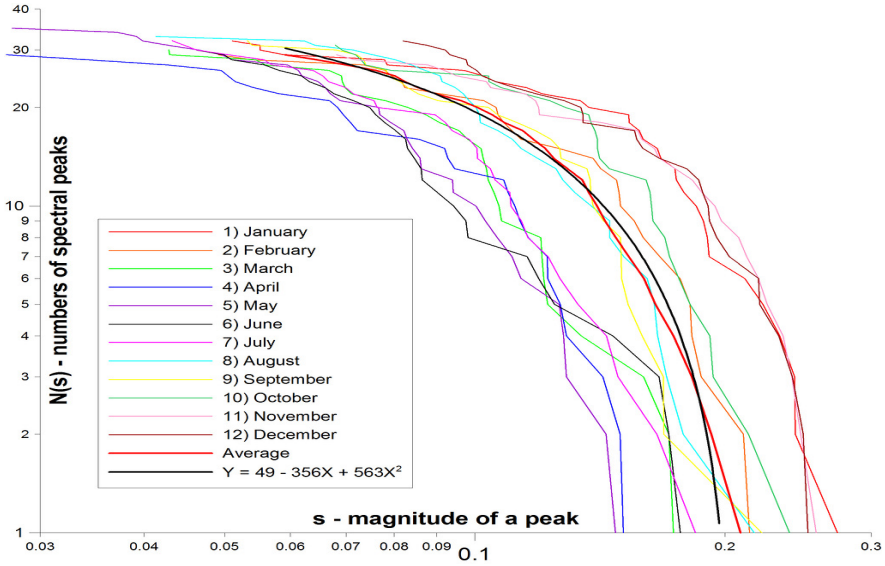

Fig. 3 Graphs of the interrelations between the magnitudes of the power spectra peaks shown in Fig. 2 and their serial numbers. The approximation of the graph of the mean interrelation by a quadratic polynomial (bold line) evidences the non-chaotic character of the ENSO.

Dynamics of intrathermocline vortices in the ocean

M. Sokolovskiy, B. Filyushkin

The existence of a tongue of Mediterranean Water (MW) at the depths of 500–1500 m is a characteristic feature of the hydrological regime in the northeastern part of the Atlantic Ocean. Anticyclonic eddies filled with MW (meddies or lenses) are observed in this region. They are identified owing to their high temperature and salinity anomalies, which compensate in density, yielding nearly homogeneous meddy cores. The analysis of historical observations has showed that approximately 100 lenses can exist simultaneously in this part of the ocean. High concentration of large water volumes (> 4000 km^3 each) can be found both in the region of their origin near the Iberian Peninsula and near the Azores Frontal Zone. The latter is precisely the region, in which merging of eddies can occur to form larger lenses. The existence of long-living lenses at large distances from the region of their formation is an indirect indication of the fact that merging of lenses occurs.

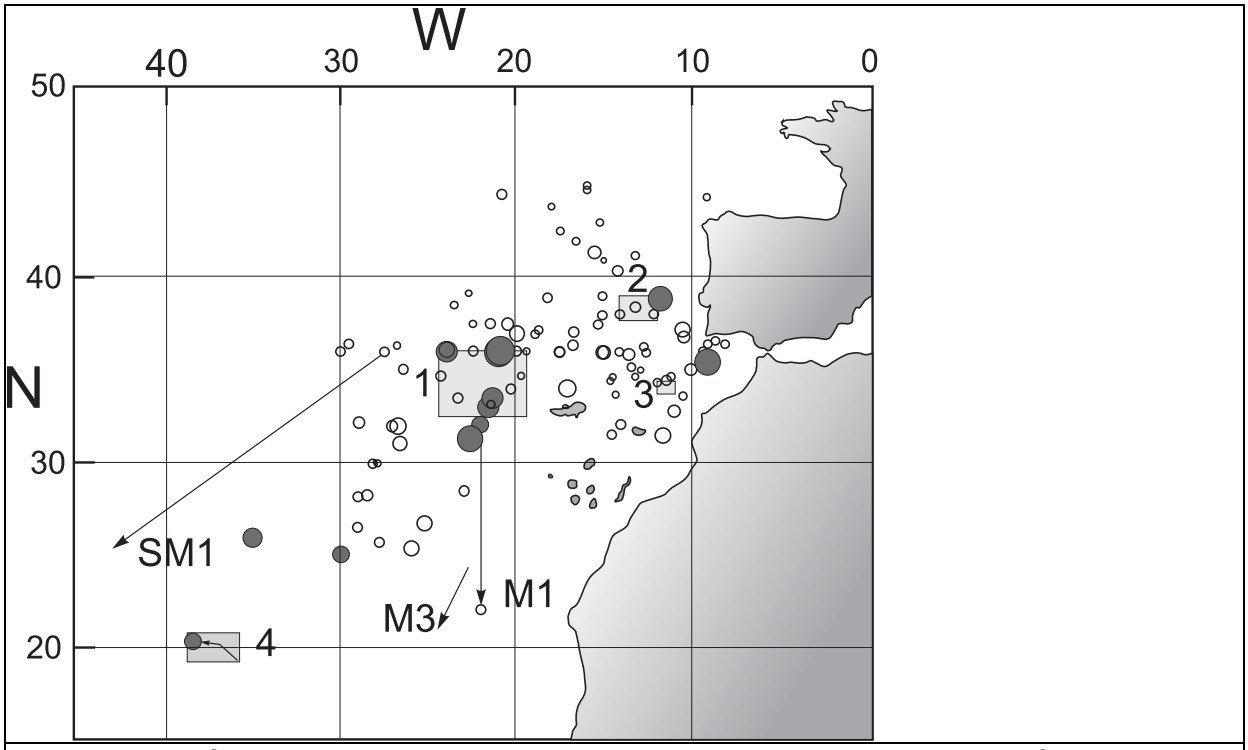

Distribution of Mediterranean lenses in the North Atlantic by the value of their volume (the size of the symbol is proportional to the lens volume). Dark color highlights the largest lenses. (1) region of the Azores Frontal Zone (Käse and Zenk 1987; Richardson and Tychensky, 1998; Tychensky and Carton 1998); (**2)** region of merging of two lenses (Schultz Tokos *et al*., 1994; Richardson *et al*., 2000); (**3)** region of the formation of a dipole lens system (Filyushkin, 1989); (**4)** Mesopolygon (Yegorikhin *et al.*, 1987), SM1 is the lens trajectory in the SEMAPHORE study region; M1, M3 are Sharon lens trajectories (Richardson *et al.*, 1989).

We analyze the results of model experiments on the interaction between two anticyclonic eddies applying the contour dynamics method (CDM) to a three-layer ocean. In these experiments, the vertical distribution of layerwise density in the layers, the horizontal size of the eddies (assumed to be cylindrical structures), and their depth location correspond to the observed conditions in the Atlantic Ocean. We show that the

evolution of intrathermocline eddies and barotropic eddies differ significantly. We found that the behavior of interacting eddies in the middle layer depends on the Froude number. We determined the critical distances between the lenses when their merger begins and the destruction' criterion for the elliptical intrathermocline eddies.

The interaction of meddies with a complex distribution of seamounts is studied in a three-layer quasi-geostrophic model on the f-plane. This study aims at understanding if and how this seamount chain can represent a barrier to the propagation of these eddies and how it can be involved in their decay. The eddies are idealized as vortex patches in the middle layer, interacting with a regional cyclonic current and with ten idealized seamounts. The numerical code is based on the contour surgery technique.

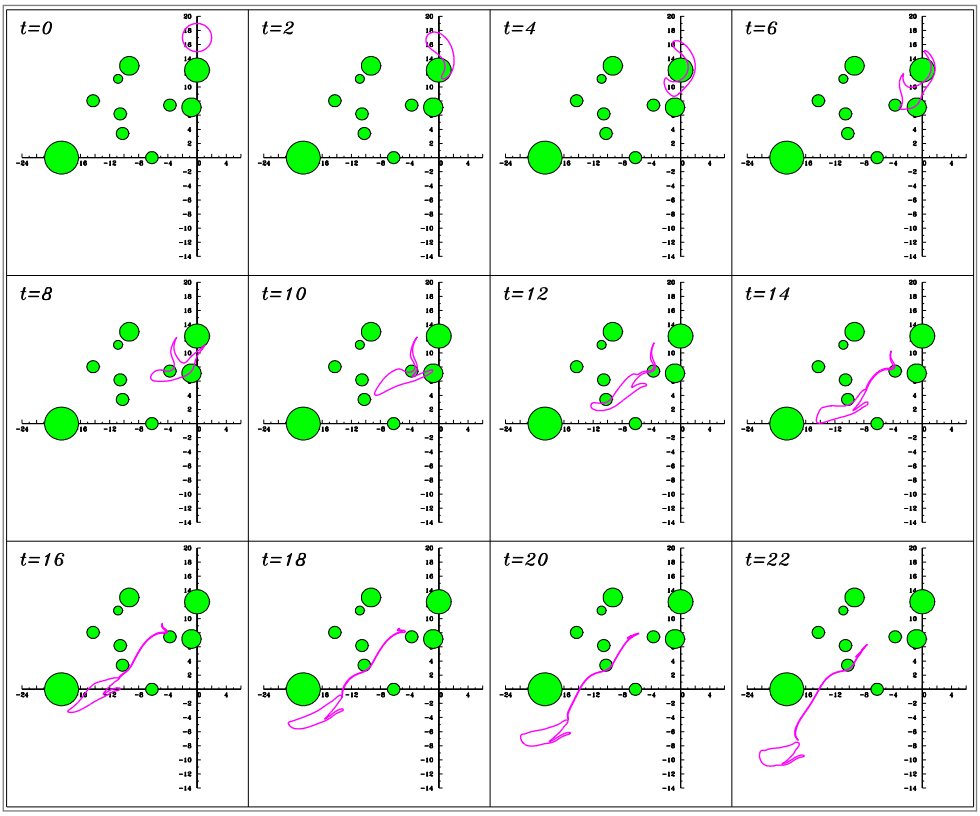

Fig. 2

This figure shows the results of interaction of meddy (solid lines) with seamount chain (dark circles), when the initial anticyclonic vortex is circular. Such a vortex crosses the seamount chain without much alteration: after the interaction with seamounts, it has lost only 0.32% of its volume; 91.17% of this volume is concentrated in a relatively compact core and 8.51% – in the filaments.

A model of ice cover evolution in the Barents Sea

A. Rodionov

A numerical model was developed to calculate the ice cover in the Barents Sea throughout the year. Only in 2006, the model had deviations from the observations. The maximum ice cover was found in 2003 and the minimum in 2002.

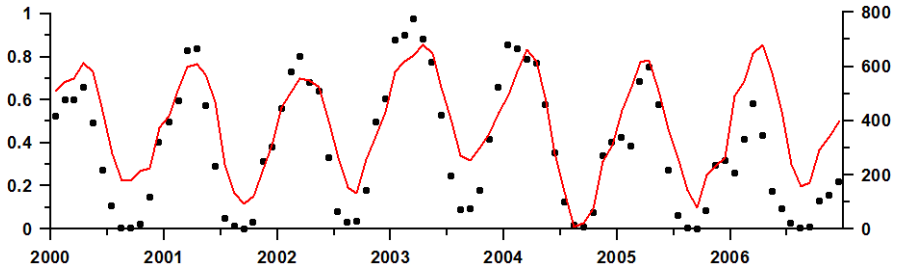

Evolution of the square of ice cover in the Barents Sea. Black dots show monthly mean values in th. sq. km (right scale) based on the data of radar imaging SSMR-SSM/I, the red line shows the calculations as the ratio of the ice covered sea to the total square (left scale).

The calculations analyzed also the temperature variation in the upper 200-m layer. The temperatures vary between the coldest and warmest years in the range 2.5–3°C. The maximum variations were found in winter in the central and southern parts of the sea. The amplitude of fluctuations at 200 m decreases by 1°C compared to the surface. Salinity fluctuations are small.

Climatic variability of hydrometeorological parameters in the Russian seas in 1979-2011

A. Kostianoy

Seasonal and interannual variability of air temperature, atmospheric precipitation, wind speed, sea level, sea surface temperature, ice cover, salinity, and river runoff duirng the period from 1979 to 2011 and water areas of all the Russian seas were studied. Linear trends and interannual variability of the increase and decrease in the investigated parameters were calculated. The analysis was performed on the basis of monthly datasets accumulated in the NASA Goddard Earth Sciences Data and Information Services Center with a spatial resolution of 1 degree. The GPCP Version 2.2 Combined Precipitation Data base and TRMM Online Visualization and Analysis System (TOVAS) were used for investigation of the accumulated precipitation in the period between January 1979 and December 2010. The analysis and visualization of the results were done with the help of the Giovanni online system elaborated by the NASA Goddard Earth Sciences Data and Information Services Center. Seasonal and interannual variability of the Black, Azov, Caspian and White seas level was investigated on the basis of altimetry data from the TOPEX/Poseidon and Jason 1/2 satellites. Several examples are shown below.

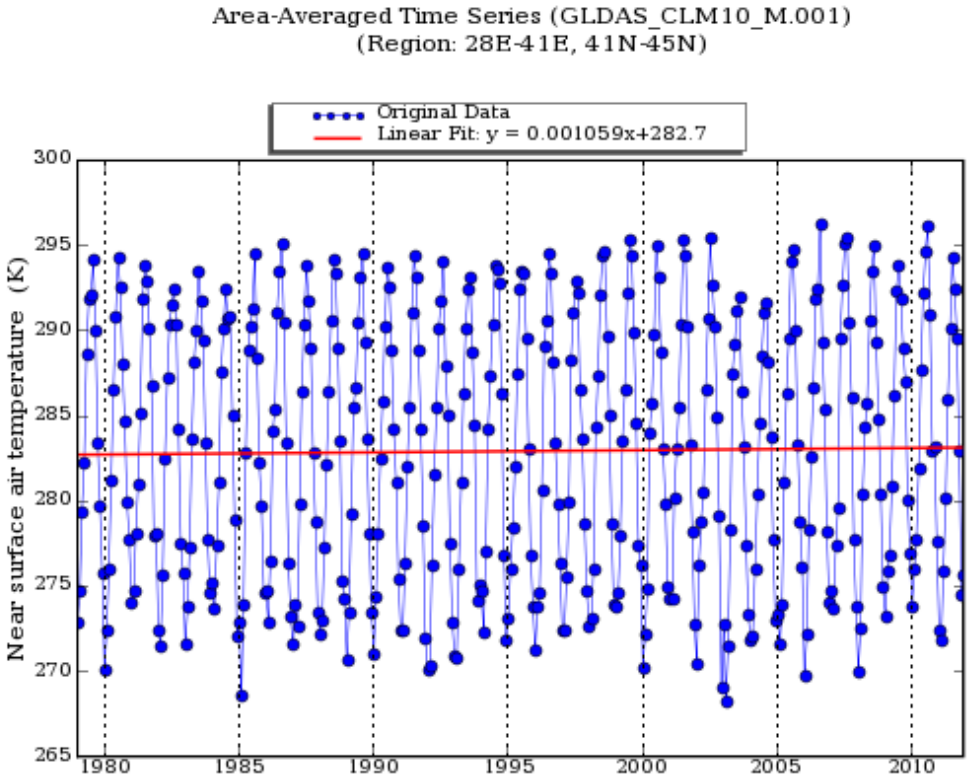

Fig. 1. Seasonal and interannual variability of the monthly mean air temperature (ºK) over the Black Sea (41–45ºN, 28–41ºE) in 1979–2011 (NASA, Goddard Earth Sciences Data and Information Services Center, Giovanni, http://disc.sci.gsfc.nasa.gov/giovanni).

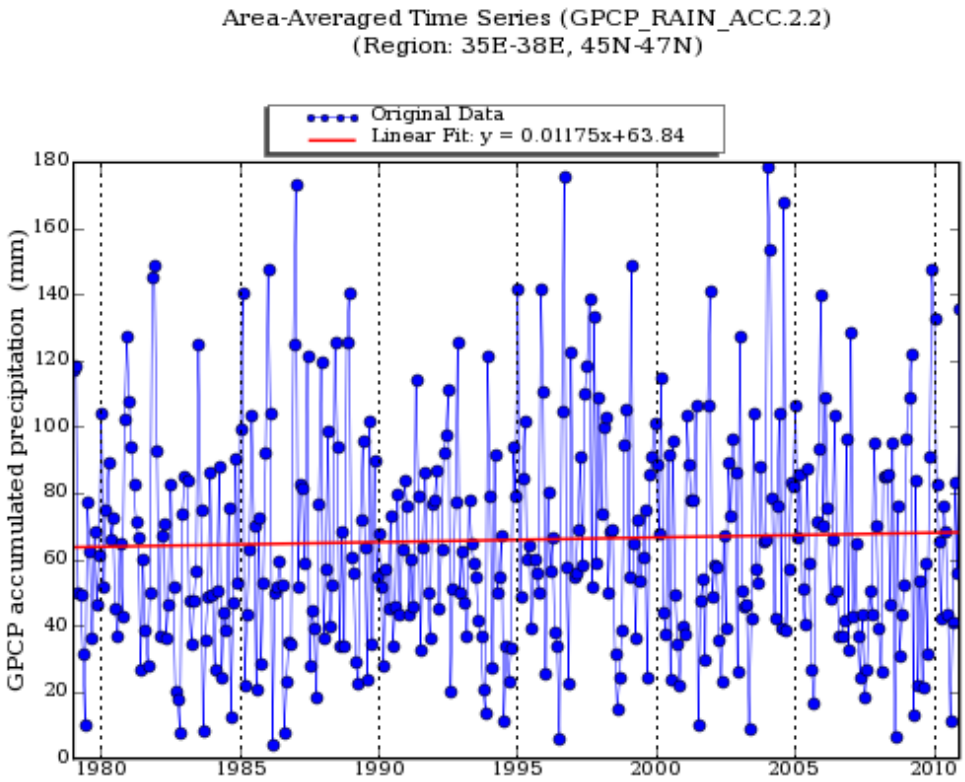

Fig. 2. Seasonal and interannual variability of monthly mean atmospheric accumulated precipitation (mm) over the Sea of Azov (45–47ºN, 35–38ºE) in 1979–2011 (NASA, Goddard Earth Sciences Data and Information Services Center, Giovanni, GPCP Version 2.2 Combined Precipitation Data, http://disc.sci.gsfc.nasa.gov/giovanni).

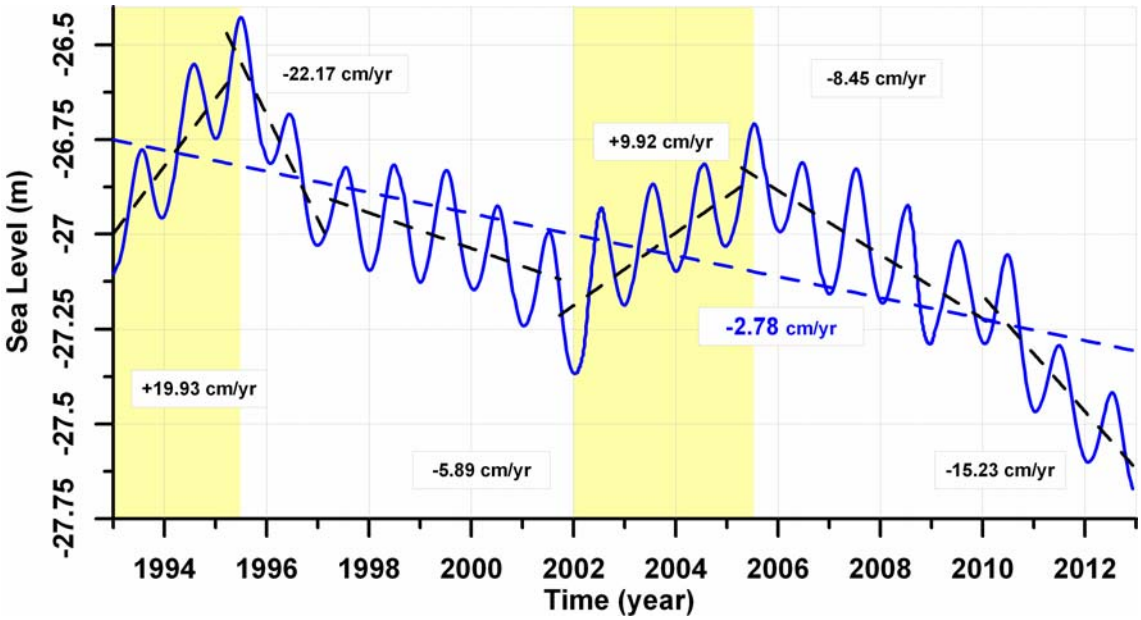

Fig. 3. Seasonal and interannual variability of the Caspian Sea level based on the Topex/Poseidon and Jason-1/2 satellite data from January 1993 to December 2012.

Table. Linear trends in the long-term variations of air temperature, precipitation, and wind velocity in the Arctic seas of Russia. The increments are related to 1979.

Sea	Air temperature 1979–2011	Precipitation 1979–2010	Wind velocity 1979–2011
Barents Sea 69–80º N 25–55º E	+0,0749^{0}C/yr ΔT = +2,47^{0}C	+5,93 mm/yr ΔP = +190 mm (or +43% relative to 1979)	+0,0272 m/s·per yr ΔV = +0,90 m/s
White S 64–68º N, 33–44º E	+0,0626^{0}C/yr ΔT = +2,07^{0}C	+1,98 mm/yr ΔP = +63 mm (or +9% relative to 1979)	-0,0044 m/s·per yr ΔV = –0,14 m/s
Kara Sea 73–81º N, 65–95º E	+0,1264^0 C/yr ΔT = +4,17^{0}C	+2,28 mm/yr ΔP = +73 мм (or +24% relative to 1979)	–0,0017 m/s per yr ΔV = -0,06 m/s
Laptev Sea 73–79º N, 110–140º E	+0,1702^{0}C/yr ΔT = +5,62^{0}C	+0,91 mm/yr ΔP = +29 mm (or +12% relative to 1979)	–0,0002 m/s per yr ΔV = –0,01 m/s
East Siberian Sea 70–77º N, 145–175º E	+0,1451^{0}C/yr ΔT = +4,79^{0}C	+0,37 mm/yr ΔP = +12 mm (or +5% relative to 1979)	–0,0111 m/s per yr ΔV = –0,37 m/s
Chukchi Sea 67–74º N, 180-156º W	+0,0679^{0}C/yr ΔT = +2,24^{0}C	–0,38 mm/yr ΔP = –12 mm (or –3% relative to 1979)	+0,01 m/s·per yr ΔV = +0,33 m/s

Properties of sea basins near the mouths of rivers at the Russian coast

P. Zavialov

We analyzed long-term field and satellite observations in the shelf regions adjacent to small Russian rivers of the Caucasian coast: Mezyb, Pshda, Vulan, Tuapse, Bitha, Sichi, Kudepsta, Mzymta). In the context of anthropogenic and terrigenous impacts we consider water properties: nitrates, phosphates, silicates, alkalinity and pH, as well as mineral and organic suspended matter and chlorophyll “a”. Special attention was focused on the plume of the Mzymta River near Sochi where the measurements have been repeated since 2007.

We observed clearly manifested river plumes in the surface layer 1-4 m thick. Usually they had clearly pronounced boundary especially on the windward side Salinity and density in the plumes were lower than in the ambient waters. Concentrations of dissolved organic compounds and chlorophyll in the plumes were increased, as well as concentrations of nutrients.

The table presents mean characteristics of plumes average over several years of measurements.

River	Mean discharge, m^3/s	horizontal scale, km	vertical scale, m	salinity anomaly, psu	suspended matter concentration anomaly, mg/l
Mzymta	49.5	3.0±1.8	2.6±1.2	3.1±1.4	25.5±17.3
Sochi	16.1	2.2±1.2	1.9±1.5	2.4±1.0	3.0±2.1
Tuapse	12.8	1.8	2.0	1.1	24.0
Pshada	9.8	1.3±0.7	0.9±0.7	0.2±0.1	0.8±0.3
Vulan	6.4	1.2±0.6	0.6±0.5	0.2±0.1	0.9±0.4
Mezyb	3.9	0.4	0.1	0.05	
Kudepsta	3.4	0.9±0.7	1.0±0.8	1.1±0.8	9.3±8.3
Bikhta	0.3	0.08	0.4	0.1	

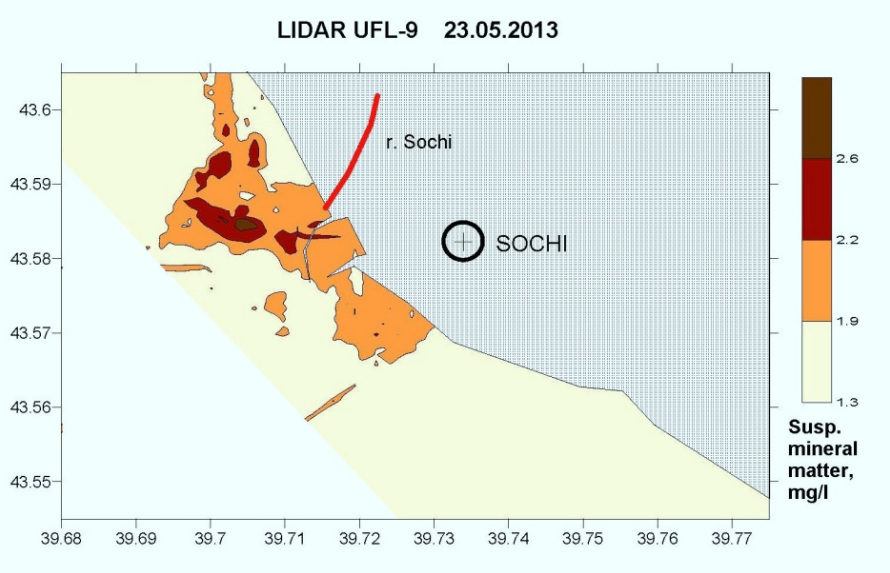

Sochi River plume in the Black Sea as manifested in suspended matter concentration from high resolution UV lidar measurements. May 23, 2013.

Aerial photo of the Mzymta mouth area and the river plume. City of Sochi, the Black Sea, spring 2013.

The Black Sea dynamics and its impact on the ecosystem studies.

Kubryakov A.A., Stanichny S.V. and Zatsepin A.G.

The general features of the Black Sea circulation are the cyclonic Rim Current, the axis of which is in located generally over the continental slope, western and eastern cyclonic gyres in the open sea. Mesoscale circulation includes coastal anticyclonic eddies, which are formed between the Rim Current and the coast and move in the cyclonic direction, and open sea eddies, both anticyclonic and cyclonic.

It was revealed that the dynamical regime of the Black Sea has changed considerably in 2002-2003. Before that time, in 1994-2002, the seasonal amplitudes of kinetic energy and its annual mean value were less than in 2003-2012. These changes were induced by the regime shift of the large-scale wind forcing. In 1994-2002 the seasonal amplitudes of wind stress vorticity and its mean annual value upon the Black Sea were considerably less, than in 2003-2011. Moreover, the seasonal variability of the Black Sea differs strongly from year to year, that is also depended on the changes in the seasonal variability of the wind stress vorticity. The interannual variance of the Black Sea circulation after 2003 shows enough clear biannual signal which can be related to the air-sea coupled interactions.

The mesoscale circulation experienced strong changes after 2002-2003. It was revealed that the variability of the mesoscale eddy energy is opposite to the mean kinetic energy of the Black Sea circulation because the weakening of the Rim current leads to its instability and the formation of the mesoscale anticyclones, while the strengthening of the Rim current suppresses the instability and mesoscale eddy formation. Thus, the total mesoscale eddy energy decreased after the intensification of the basin-scale circulation in 2002-2003, and the total number of eddies reduced. At the same time, the intensity of the recurrent anticyclones such as the Sevastopol and Batumi eddies increased significantly, especially in the spring months.

The decrease of the chlorophyll “a” concentration after 2002-2003 is related probably to the reduction of the eddy induced horizontal transport of the rich coastal waters to the deep part of the basin. This reduction is a result of more organized basinscale circulation, decreasing number of mesoscale eddies, and intensification of the frontal barrier between the coastal and open sea waters. Thus, the chlorophyll “a” concentration decrease occurs in the deep part of the basin. At the same time, the intensification of the Rim current leads to the increase of the chlorophyll “a” concentration in the shelf zone, especially along the coast from the Danube mouth to the Bosporus Strait due to transport of nutrient-reach Danube waters. The obtained result contradicts with the wide spread opinion that the intensification of the basinscale circulation leads to an increase of winter-spring phytoplankton blooming in the central part of the Black Sea.

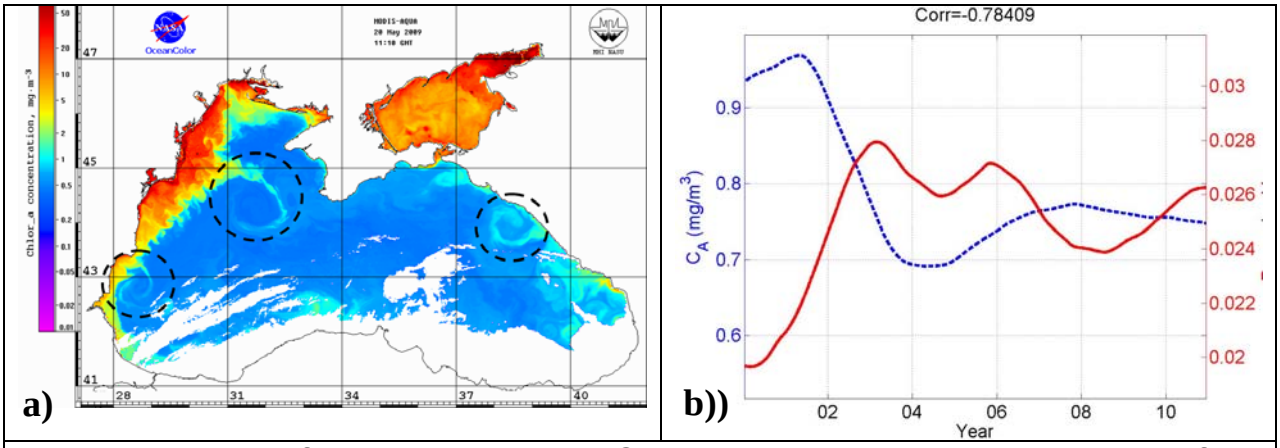

Fig.1. The impact of lateral advection on Cla_a concentration in the central part of the Black Sea: a) MODIS-Aqua Cla_a concentration image illustrating the eddy induced advection of Cla_a and nutrients from the periphery of the basin to its central part; b) negatively correlated variability of CLa_a concentration (blue line) and specific kinetic energy of mean currents during 1998-2011.

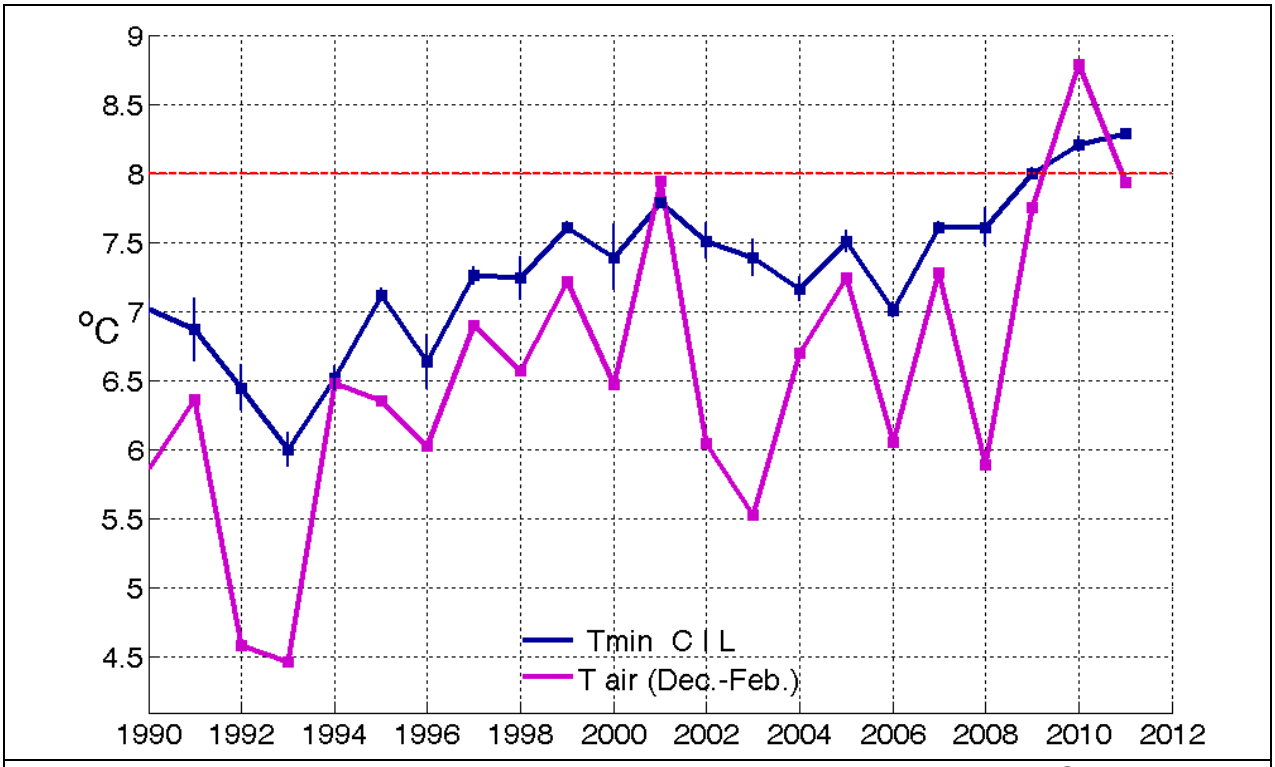

Fig. 2. Mean winter (December-February) air temperature over the Black Sea (violet line) and a minimal temperature of Cold intermediate layer (CIL) core (blue line) in the north-eastern part of the Black Sea in summer-autumn seasons.

Unsteady overflow in the Słupsk Furrow of the Baltic Sea

V. Zhurbas

The Słupsk Furrow, a channel-like topographic constriction in the southern Baltic Sea between the Bornholm Basin and the Eastern Gotland/Gdansk basins (Fig. 1), is the only pathway for salty water from the North Sea to enter the deep basins of the Baltic Proper and ventilate them laterally. A data set of closely spaced CTD profiling performed aboard Russian and Polish research vessels from 1993–2009, and numerical modeling are applied to study the variability of salinity(density) and velocity fields in the Słupsk Furrow overflow. The numerical simulations show that, on the one hand, the overflow may be treated dynamically within the Furrow as a subcritical, eddy-producing gravity current with the Froude and Ekman numbers in the range of $\mathrm{Fr} = U(BH)^{-1/2}$ =0.2–0.4, $\mathrm{Ek}_1 = (u_*^2 f^{-1} U^{-1})/H$ =0.04–0.08, and $\mathrm{Ek}_2 = (0.4\,u_* f^{-1})/H$ =0.5–0.8, where *U*, *B*, and *H* are the overflow's velocity, buoyancy jump and depth, respectively; u_* is the bottom friction velocity. On the other hand, the gravity current displays some features at the sill peculiar to frictionally controlled rotating flows with the Ekman numbers in the range of $\mathrm{Ek}_1 = 0.2$–0.4 and $\mathrm{Ek}_2 = 1.5$–3.0. Comparison between the field measurements and the simulation results indicates that the variability of the cross-channel density structure is caused mainly by meandering of the gravity current and mesoscale eddies – mostly overlying cyclones and neighbouring anticyclones (Fig. 2). The meanders and eddies are found to be affected strongly by the bottom topography and wind forcing.

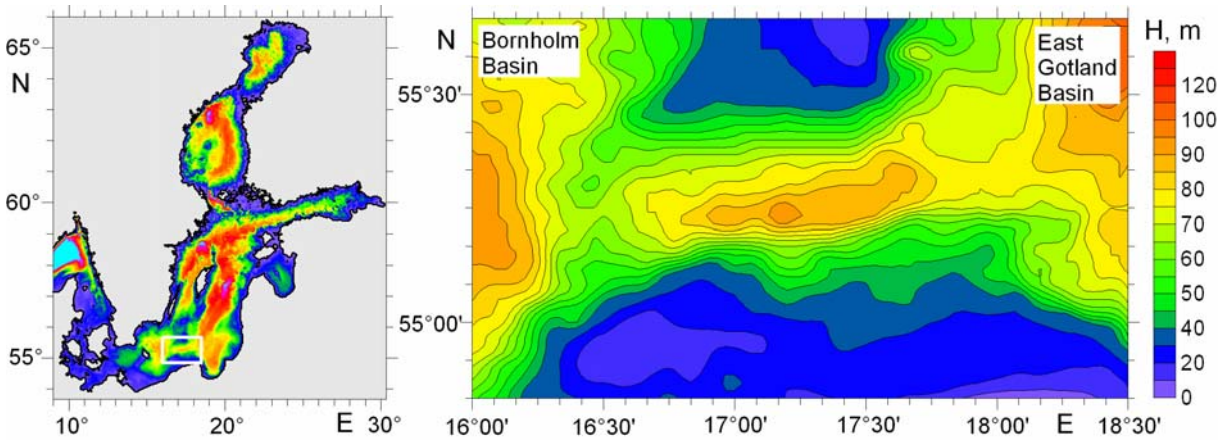

Fig. 1. Bathymetric map of the Baltic Sea (left) and close-up of the Słupsk Furrow (right).

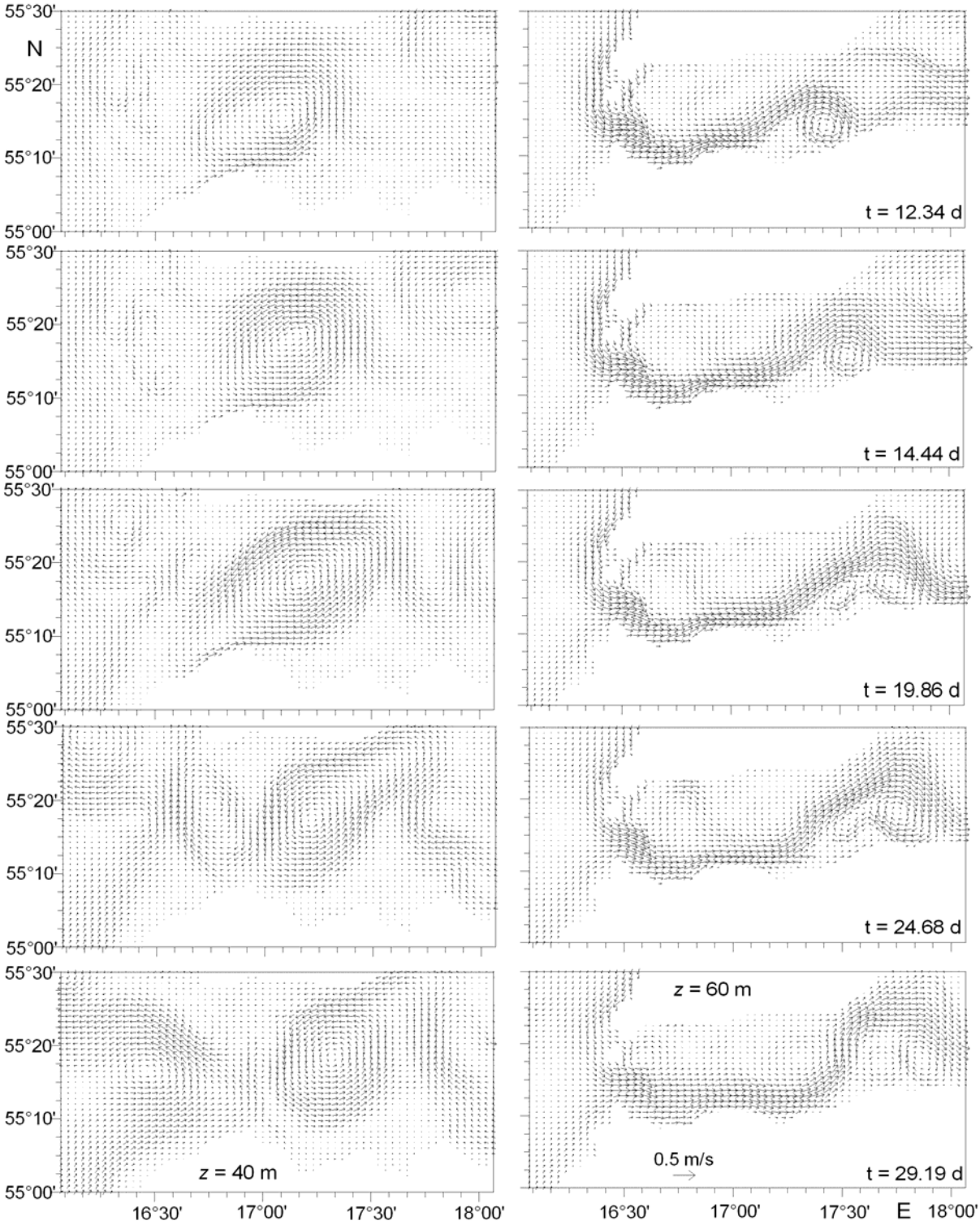

Fig. 2. Snapshots of simulated current velocity in the Słupsk Furrow at 40 m and 60 m depth presented for different points of time. The snapshots clearly display meandering of the gravity current as well as generation of neighbouring anticyclonic eddies (right panels) and overlying cyclonic eddies (left panels).

Variability of circulation and eddy kinetic energy in the Japan Sea (from satellite altimetry)

O. Trusenkova

Several statistically significant and physically meaningful variability patterns of sea level (SL) and eddy kinetic energy (EKE) in the Japan Sea are detected by means of multivariate analysis of satellite altimetry data. The analysis was complicated by the strong seasonal signal featuring the SL rise in the warm season and decline in the cold season in the entire Sea (in-phase SL oscillations), with the seasonal extremes in October and March, respectively. The newly detected patterns are as follows.

The SL Gradient Mode captures strengthening and weakening of the meridional SL gradient across the Subarctic Front (Fig. 1) which occurs simultaneously with the in-phase SL oscillations. This means the circulation strengthening in the warm season and weakening in the cold season, with the seasonal extremes in October and March, respectively, unlike the wind-driven oceanic gyres but being linked to the seasonal variation of the warm water inflow in the Korea Strait.

The EKE Instability Mode is spatially linked to the zones of the mean boundary currents and bathymetric features in the Japan Sea (Fig. 1), although mean EKE in the subarctic (northern) area is an order of magnitude smaller than that in the subtropical (southern) area. This is consistent with the acknowledged mechanisms of EKE generation, such as dynamic instability and flow interaction with bathymetry. EKE in the entire Japan Sea increases in the warm season and decreases in the cold season, with the seasonal extremes in October to November and in March to April, respectively. Baroclinic instability is usually considered as the EKE source, however, the same seasonal variation of EKE and mean currents, whose possible effect on EKE has been removed, implies a strong impact of shear instability.

The EKE Primorye mode accounts for EKE variability in the subarctic area off the Russian (Primorye Province) coast (Fig. 1). Seasonal variation is similar but less regular than that of the EKE Instability mode and the annual, quasi-biannual, and 5–6-year time scales are detected (Fig. 2a). As the broad spatial maximum is not linked to either hydrographic or bathymetric features, wind forcing of EKE off the Primorye coast is suggested.

The coupled SL and EKE patterns are revealed which represent **the East – West Seesaw** between pathways of warm water transport from the Korea Strait northward (Fig. 3). In the positive phase (late summer on the seasonal time scale) northward advection of warm water is intensified in the eastern Sea – within the meandering Tsushima Warm Current along the Japanese Islands. In the negative phase (from autumn through early summer, weakening in winter) anticyclonic circulation intensifies in the western Sea, including mesoscale eddy formation in the northwestern area. This seesaw evolves on the semiannual, annual, quasi-biennial, and 5–6 time scales, the latter representing the regimes of the prevailing positive or negative phase (Figs. 2b, 3b). Wind-driven circulation changes are suggested as the forcing.

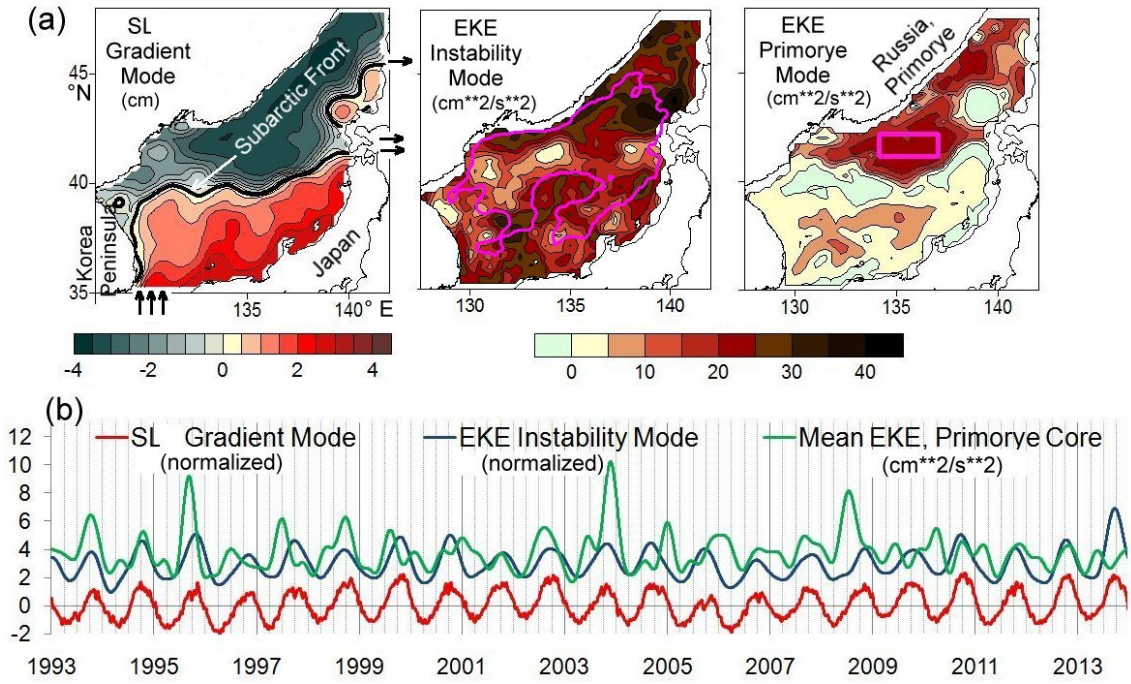

Fig. 1. (a) Spatial patterns and (b) temporal variability of the SL Gradient Mode and EKE Instability and Primorye Modes in the Japan Sea, derived from satellite altimetry data. Temporal variability of the Primorye Mode is represented by mean EKE (cm^2/s^2) off the Primorye (Russia) coast. (a, left panel) The inflow in the Korea Strait and the outflows in the Tsugaru and La Perouse (Soya) Straits are marked by arrows, (a, central panel) the 2000 m isobaths is shown by magenta contour, and (a, right panel) magenta rectangular shows the area for EKE averaging.

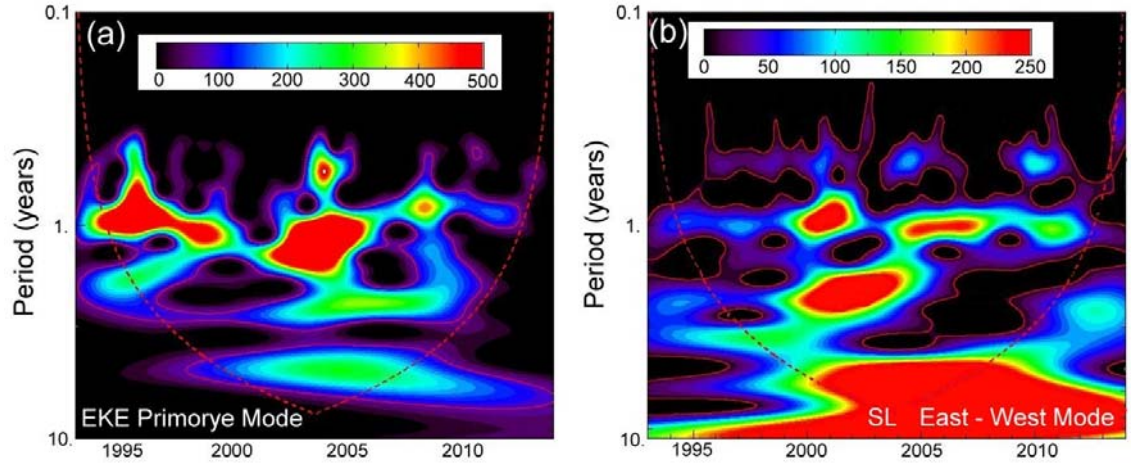

Fig. 2. Wavelet transforms (a) of mean EKE within the Primorye Mode and (b) of the normalized temporal function for the SL East – West Mode. The cone of influence and the 95% level of statistical significance, with respect to the red noise, are shown.

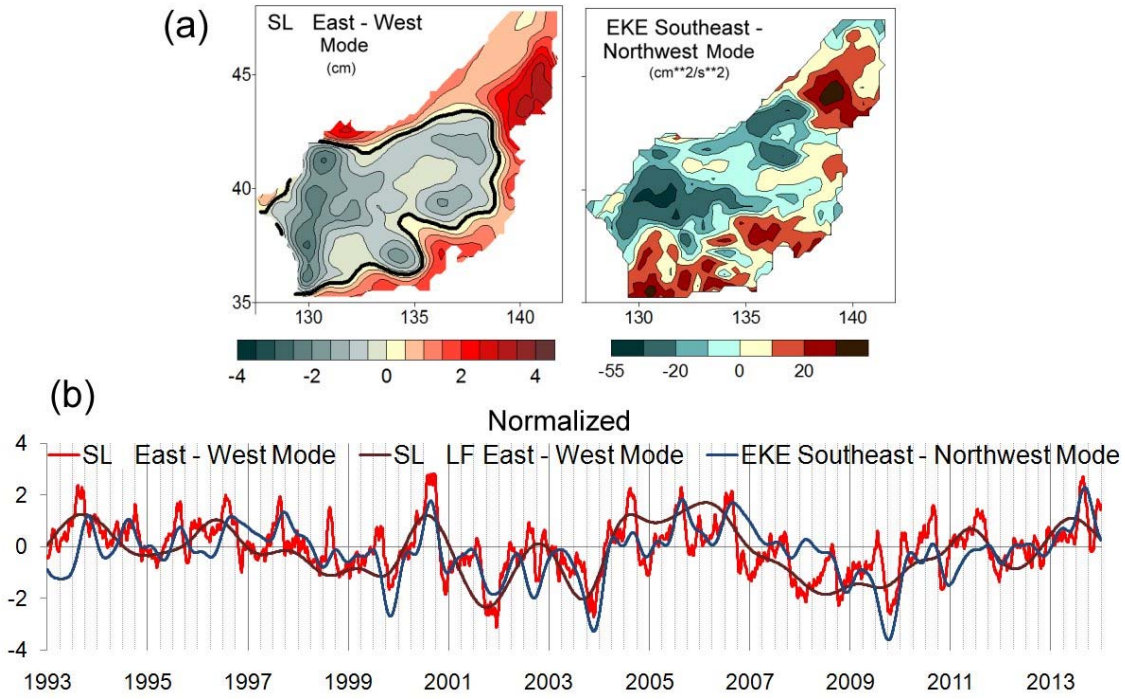

Fig. 3. (a) Spatial patterns and (b) temporal variability of the SL East – West Mode and EKE Southeast – Northwest Mode in the Japan Sea derived from altimetry data. Low-frequency (LF) temporal function of the East – West Mode is shown.

Multiple scale climatic anomalies in the Subarctic zone of the Far East seas

V. Ponomarev, E. Dmitriyeva, S. Shkorba, N. Savelyeva

Wintertime anomalies of oceanographic characteristics in the Okhotsk and Japan Seas are detected on the interannual, decadal and interdecadal time scales and their linkages with surface heat flux in the North Pacific Ocean are revealed. The strong East Asia winter monsoon resulting in the increased ice extent in the Okhotsk and Japan Seas is accompanied by the increased wintertime heat flux from the ocean to the atmosphere in the entire subarctic Pacific and in the western and eastern subtropical region (Figs. 1, 2). In this case, the net heat flux to the ocean from the atmosphere is weakened in the equatorial and tropical Pacific. Reduction of SST and net heat flux to the ocean in western subtropical and eastern subarctic Pacific during the previous warm season can be used as a predictor of cold winter conditions in the Okhotsk and Japan Seas.

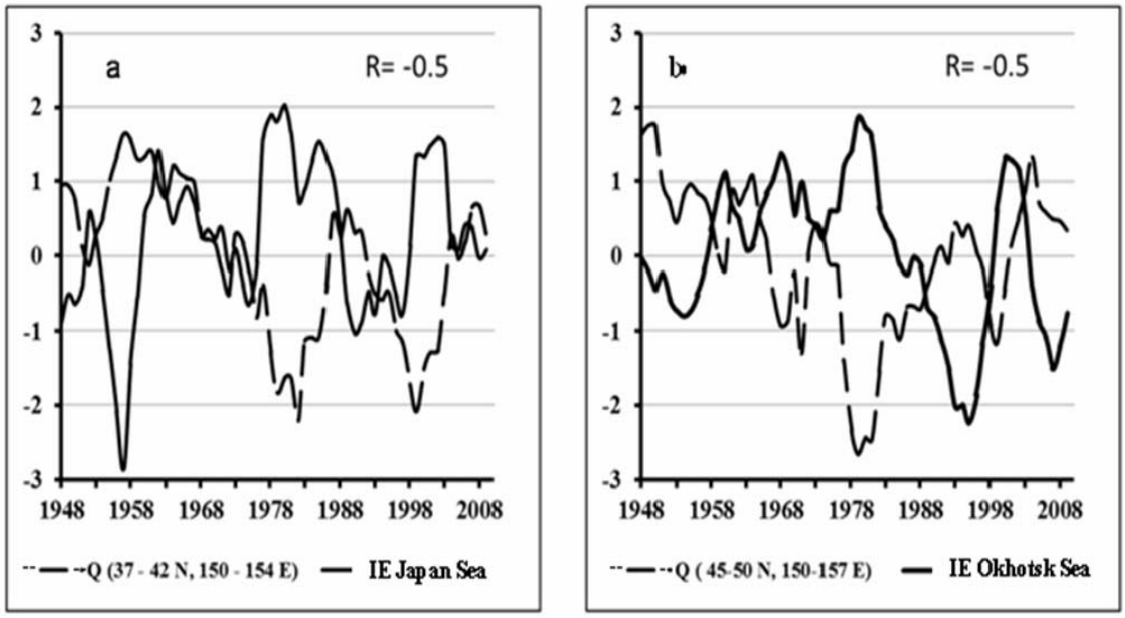

Fig.1. Normalized anomalies of the 5-year running mean ice extent (IE) in the Okhotsk and Japan Seas in February and net heat flux Q from the ocean to the atmosphere (negative values) in winter averaged within the areas of the Northwest Pacific for 1948-2012; correlation between the time series in also shown.

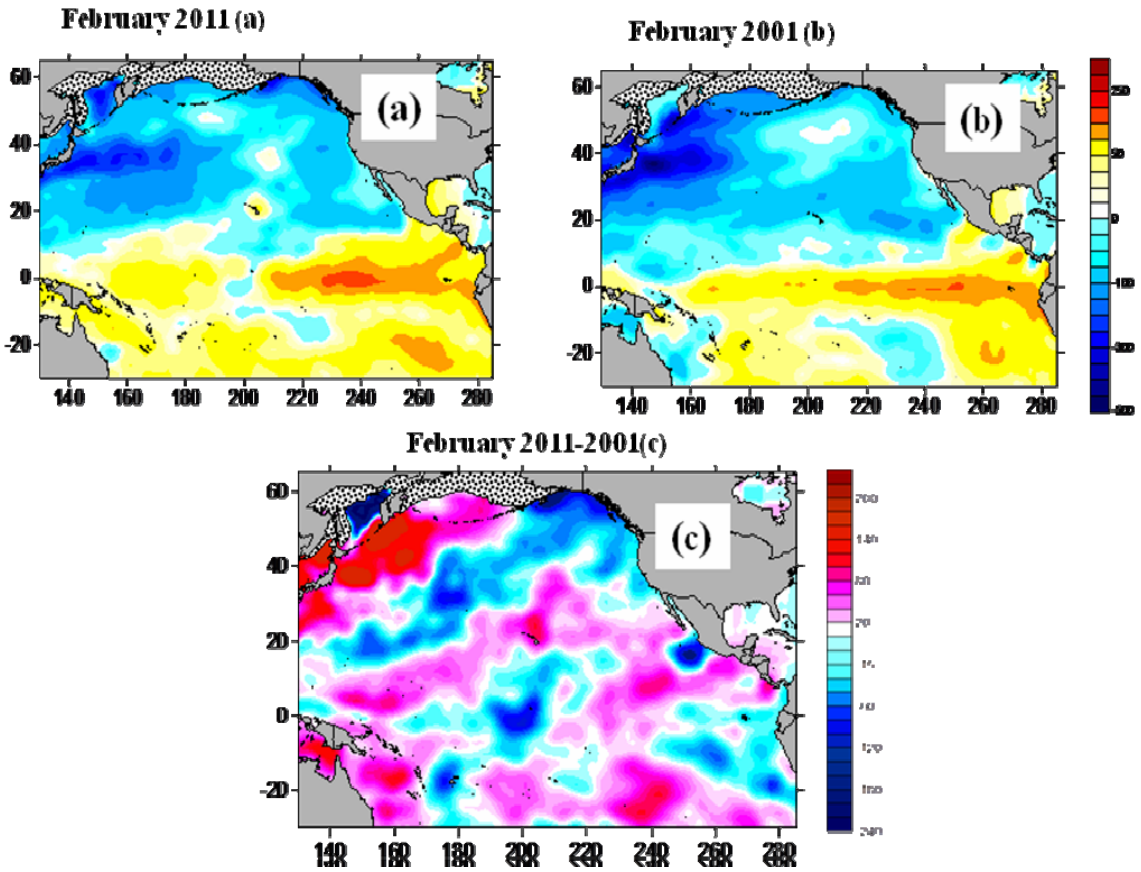

Fig.2. Net heat flux (Q, W/м^2) in February for the (a) warm conditions (2011) and (b) cold conditions (2001) derived from NCEP Reanalysis and (c) difference between (a) and (b). The heat flux is negative when directed from the ocean to the atmosphere.

Simulation of mesoscale and sub-mesoscale circulation in the northwestern Japan Sea

V. Ponomarev, P. Fayman, S. Prants, M. Budyansky, M. Uleysky, V. Dubina, I. Mashkina

Using high resolution satellite imagery and simulations with the eddy resolving oceanic model developed by N.B. Shapiro and E.N. Mikhailova, Marine Hydrophysical Institute, Sevastopol, dynamic structures on the shelf, over continental slope and in deep basin of the Northwestern Japan Sea are studied. Intra-seasonal and seasonal variability, including formation, movement, interaction, and decay of mesoscale and sub-mesoscale anticyclonic and cyclonic eddies, is revealed. On the external shelf of Peter the Great Bay, Japan Sea, activity of sub-mesoscale cyclones intensifies in fall (Fig. 1) when the surface mixed layer is deepening and seasonal pycnocline is weakening. Dimensions of sub-mesoscale cyclones vary from 1 to 12 km and those of mesoscale eddies vary from 15 to 60 km.

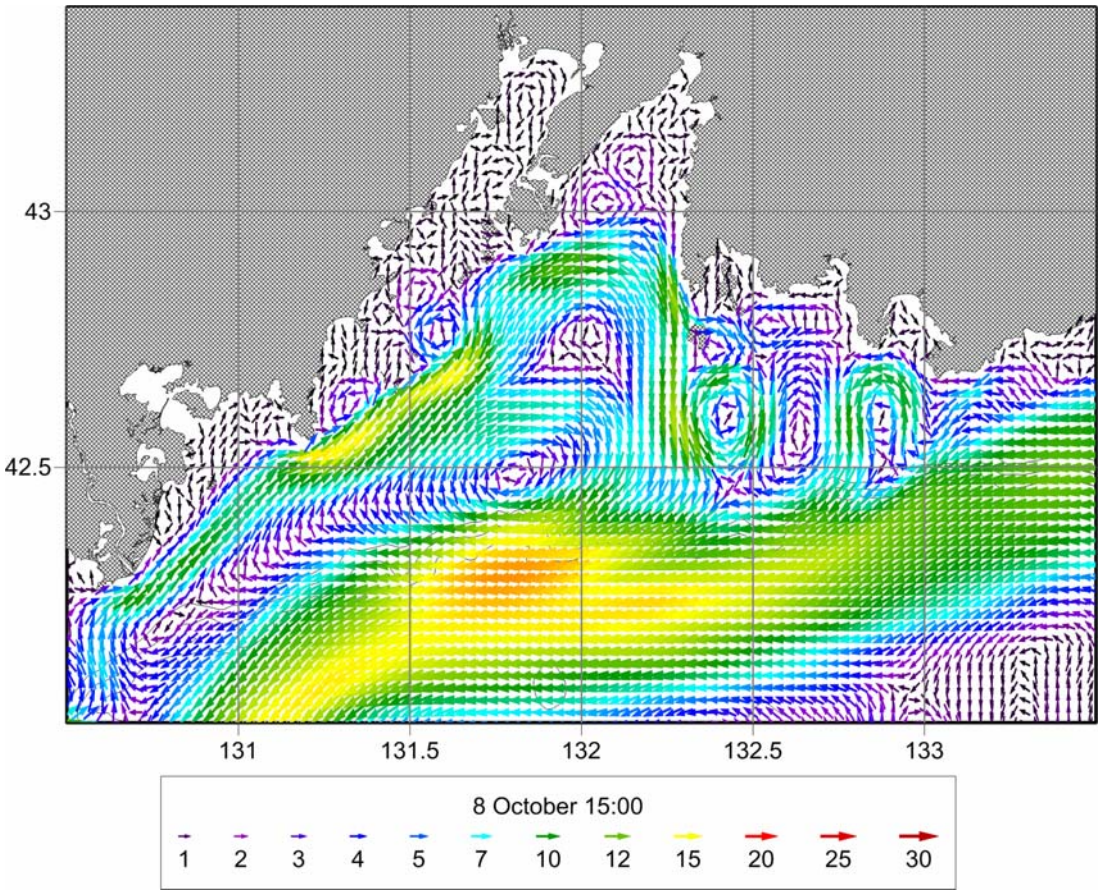

Fig. 1. Simulated currents (cm/s) in the surface mixed layer in Peter the Great Bay and adjacent deep sea area of the Japan Sea on 8 October.

The horizontal dimensions of cyclonic eddies increase with depth in the stratified flow, while dimensions of anticyclonic eddies decrease with depth which occur both in the shelf and deep sea area. Life times of sub-mesoscale cyclones generally do not exceed 2-3 days, while life times of mesoscale eddies vary from several days at the shelf edge and steep continental slope of the Japan Basin to about several months at the wide external shelf of Peter the Great Bay and longer time in central area (Fig.2) of the deep basin (Prants, Ponomarev, Budyansky, et al., 2015).

Lagrangian approach is applied to study evolution of mesoscale eddies over the continental slope, transport and mixing in Peter the Great Bay, and a topographically controlled anticyclonic eddy in the western Japan Basin. Spatial distribution of finite-time Lyapunov exponent and tracer displacements made it possible to identify pathways and barriers controlling transport and mixing at the mesoscales and submesoscales.

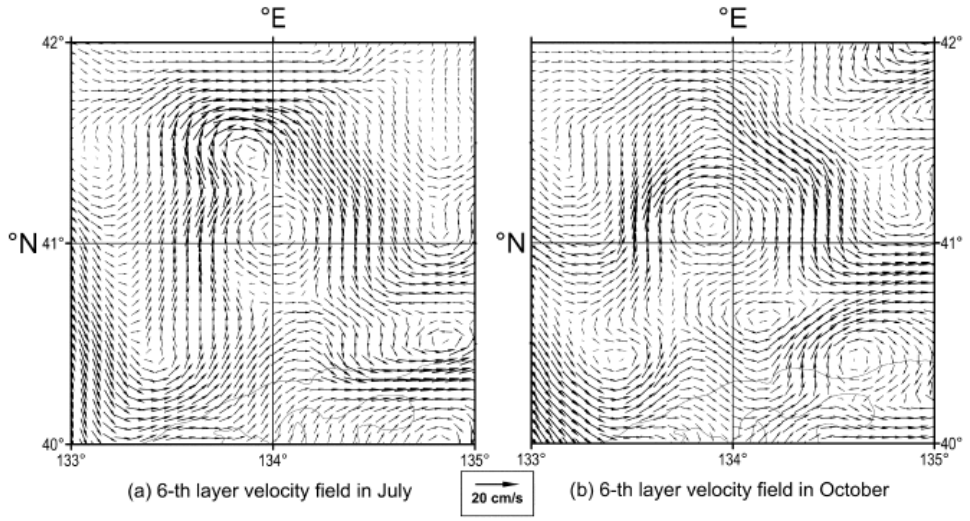

Fig.2 Currents (cm/s) in pycnocline in the central Japan Basin, off Peter the Great Bay, in (a) July and (b) October.

Coupling of Sea surface temperature and surface wind in the Okhotsk Sea and Northwestern Pacific

M. Permyakov, T. Kleshcheva

Relationship between sea surface temperature (SST) and surface wind speed and direction from QuikSCAT scatterometer and AMSR-E microwave radiometer for 2006-2009 is revealed over the Kashevarov Bank, Okhotsk Sea, and after the passage of tropical cyclones (typhoons) in the subtropical Northwestern Pacific. Surface wind speed is decreased over cold water patches in the Kashevarov Bank (Fig. 1). Moreover, occurrence of events with statistically significant SST – wind correlation manifests clear seasonal variation, with maximum of 65%-70% in September. In the Kashevarov Bank, SST anomalies can reach -10.5°C, -10.1°C, -8.2 °C and wind speed anomalies can reach -7.3 m/s, -4.8 m/s and -3 m/s for separate satellite passes and 3-day and monthly means, respectively. Coupling between SST and wind speed satisfy linear relation, with the slope of 0.3 m/s/°C and correlation of 0.5, 0.7 and 0.9 for separate passes and 3-day and monthly means, respectively (Fig. 2). The tendency towards the increased regression slope with the decreased latitude is revealed (Fig. 3). In the subtropical Northwestern Pacific SST anomalies are no more than -2.5°C and they are accompanied by wind speed anomalies of no more than -3.5 m/s in the zones of typhoon passage. SST – wind correlation remains statistically significant several days, with maximum value of 0.8 on the next day after the typhoon passage.

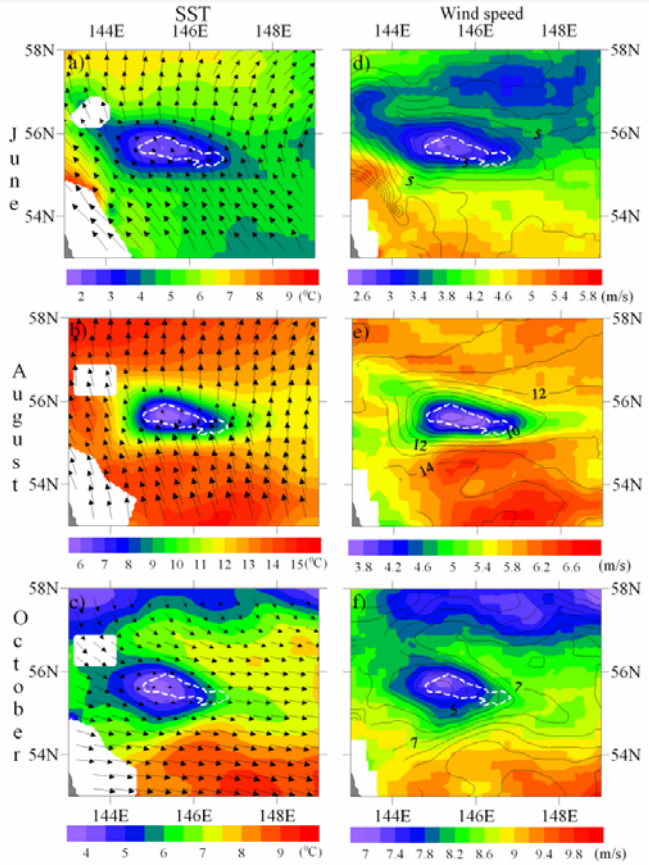

Fig. 1. Monthly mean (a-c) SST and (d-f) wind speed fields in the warm season, 2006, around the Kashevarov Bank. The area shallower than 200 m is outlined by the white contour.

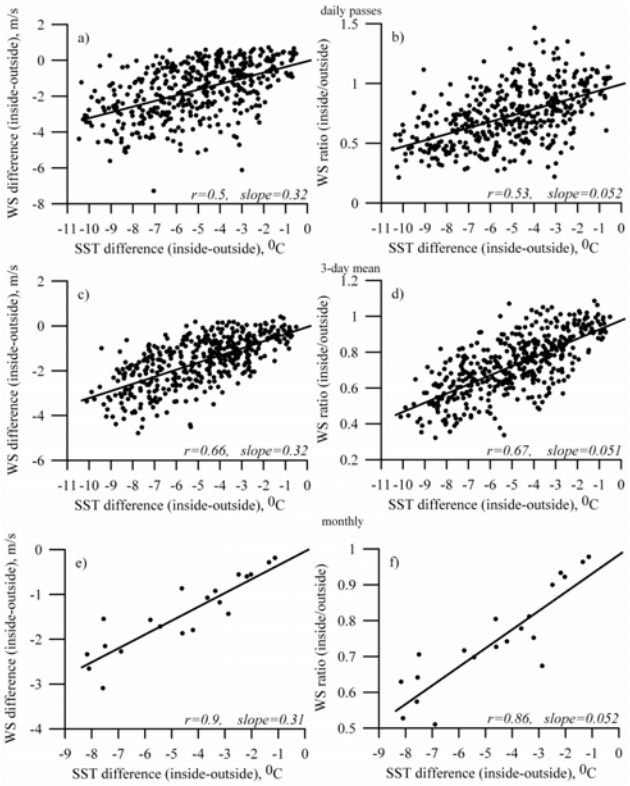

Fig. 2. Scatter plots of (left panel) wind speed (WS) and SST difference and (right panel) wind speed ratio and SST difference for (top) separate satellite passes and (centre) 3-day and (bottom) monthly means for June-October 2006-2009.

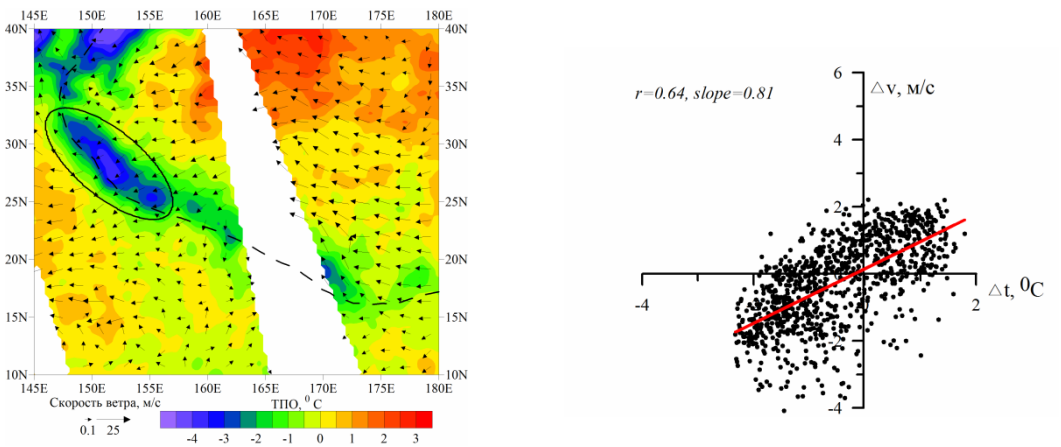

Fig. 3. SST anomalies and wind speed in the cold “wake” of typhoon Ioke and their scatter plot on September 7, 2006.

Wind waves

S. Badulin

A model of surface wave steepness was developed to estimate the steepness and of waves and their period from satellite altimetry measurements.
Wave steepness is calculated from the theory of wave turbulence.

$$\mu = 0.596 \left|\nabla H_s\right|^{1/5}$$

Here Hs is the altimetric wave height measured from satellites,
and μ is the calculated wave steepness.
We suggest a method to estimate wave steepness based on altimetric wave height and its spatial gradient. Satellite altimeter measures only the wave height but not its period and length.
The method is similar to the widely known method of estimating the current velocities from the geostrophic balance based on altimetry.
We constructed global distributions of period and wave steepness from the altimetry data.

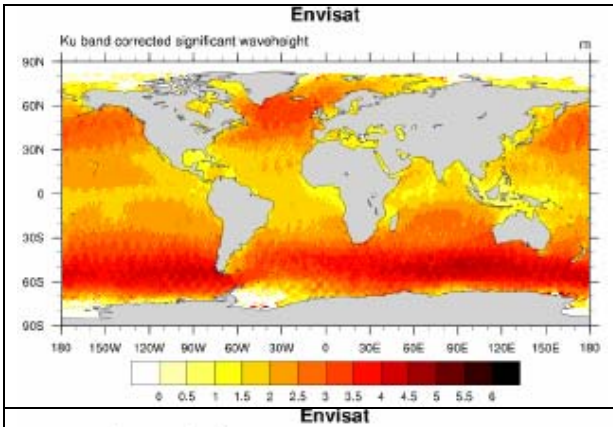	The global altimetry chart based on the satellite altimeter
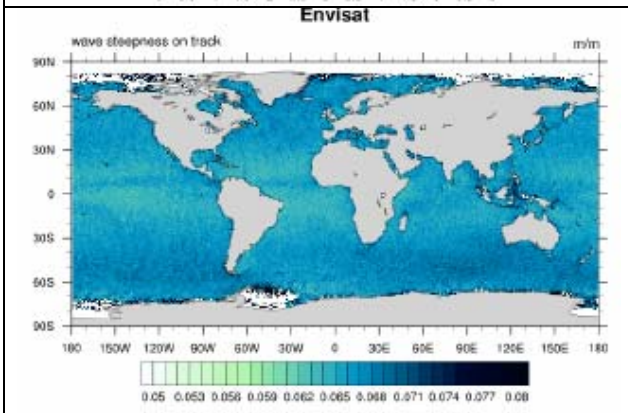	Wave steepness $\mu = \frac{\pi^2 H_s}{g T_p^2}$ is a calculated value.
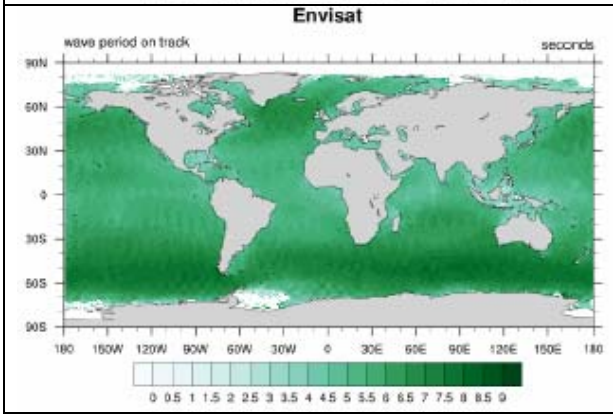	Wave period is a calculated value $T_p = 2^{1/5} \pi \alpha_{ss}^{-3/10} \sqrt{H_s / g} \left\lvert \nabla H_s \right\rvert^{-1/10};$ $\alpha_{ss} \approx 0.67$

Tsunami energy decay

E. Kulikov and A. Rabinovich

The 2009 Samoa (M_w 8.1), 2010 Chile (8.8), 2011 Tohoku (9.0) and 2012 Haida Gwaii (7.7) earthquakes generated destructive trans-oceanic tsunamis, which were recorded by a great number of open-ocean stations and coastal tide gauges in the Pacific Ocean. The high-quality data from these instruments were used to examine the physics of tsunami generation and propagation, in particular the tsunami energy decay. The numerical model of the 2011 Tohoku tsunami was initialized with the results from a seismological finite fault model and validated using deep-ocean bottom pressure records, as well as data from four satellite altimetry passes. Based on statistical analysis of the available observations and the numerical model, the authors [*Fine et al*., 2013] could demonstrate that the temporal evolution of tsunami wave energy in the Pacific Ocean leads to the wave energy equipartition law. They also showed that the long-term near-equilibrium state is governed by this law: after the passage of the tsunami front, the tsunami wave energy density tends to be inversely proportional to the water depth, i.e. that the tsunami wave intensity is simply energy density times the depth. This wave intensity fills the Pacific Ocean basin uniformly, except for the areas of energy sinks in the Southern Ocean and Bering Sea. Also the evolution of tsunami signal variance in the deep ocean clearly shows two processes: the initial decrease in the variance during the first 1–1.5 days changes into a more gradual decrease during the following days. The initial decrease is obviously related to the spreading of tsunami energy, i.e., diffusion, while the subsequent decrease is related to physical dissipation (Fig.1).

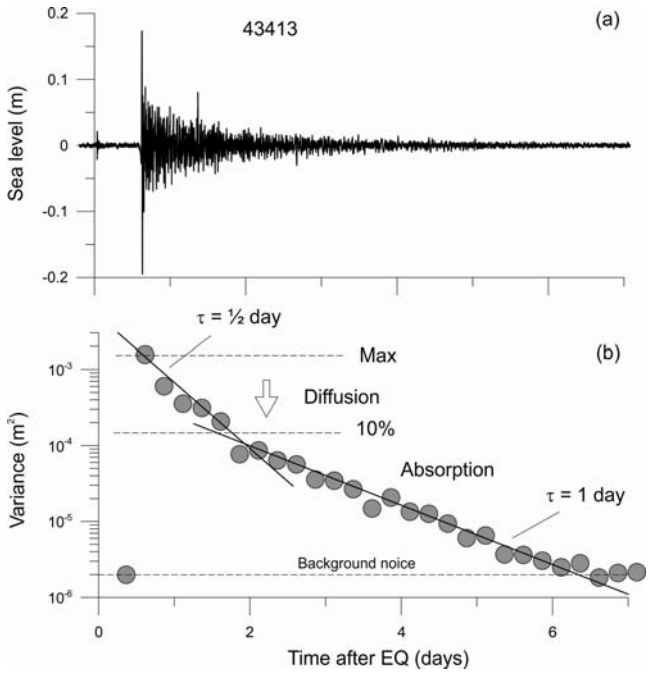

Fig. 1. Tsunami record from DART 43413 and b sea level variance change with time. The variance was calculated over a moving 6-h window. Solid lines show exponential approximation of the variance change $\sim e^{-t/\tau}$, where τ is a decay time scale. Horizontal dashed lines mark the observed maximum, the 10 % of the maximum and the level of background noise (~ 2 10^{-6} m^2)

High-resolution (15-sec) open-ocean DART records of the 2009 Samoa, 2010 Chile and 2011 Tohoku enabled *Rabinovich et al.* [2013] to estimate the mean energy decay times (τ) for these events of 17.3, 24.5 and 24.6 hrs, respectively (Fig.2). The differences in the decay times were attributed to the differences in the frequency content of the corresponding tsunamis. Specifically, the Samoa tsunami was a "high-frequency" event with periods of 2-30 min whereas the Chile and Tohoku tsunamis were "broad-band" events with periods of 2-180 min. Differences in frequency content are linked to differences in the source parameters: Samoa was a relatively small deep-water earthquake while Chile and Tohoku were extensive shallow-water earthquakes. Frequency-dependent analysis of the Chile and Tohoku tsunamis indicated that shorter period waves attenuate much faster than longer-period waves (decay times range from 15 hrs for 2-6 min waves to 29 hrs for 60-180 min waves). The authors showed that relatively small-scale, high-frequency tsunami wave components are absorbed more actively and decay more rapidly than larger-scale lower-frequency wave components. The results of the study support this idea and can account for markedly different decay times for the 2009 and the 2010-2011 tsunamis

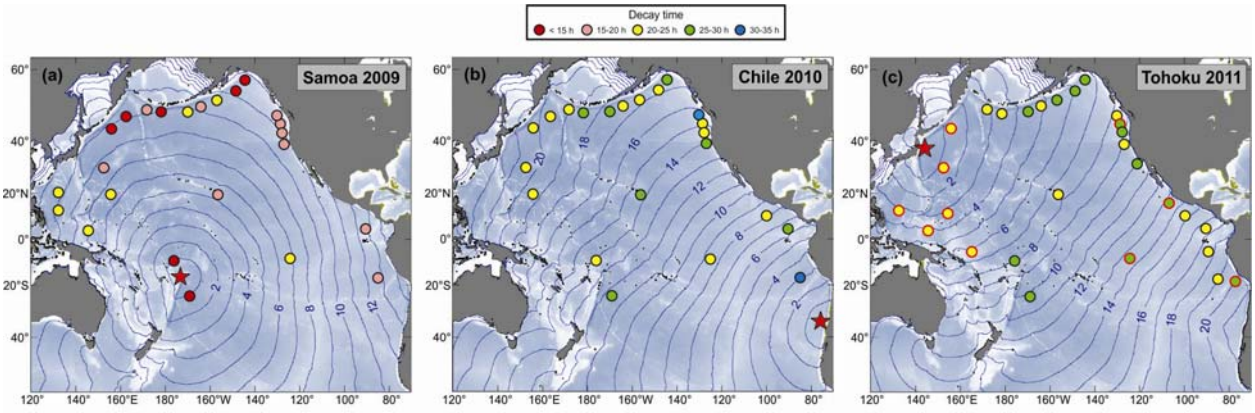

Fig. 2. The energy decay times, τ, for the: (a) 2009 Samoa; (b) 2010 Chile; and (c) 2011 Tohoku tsunamis. of the three tsunamis. Positions of the DART buoys are indicated by colour circles; colours denote the tsunami decay time. Red stars indicate the earthquake epicenters. Solid thin blue lines are hourly computed isochrones of tsunami travel time from the source areas.

Stochastic modeling of rogue waves

A. Slunyaev, A. Sergeeva, E. Pelinovsky, I. Didenkulova

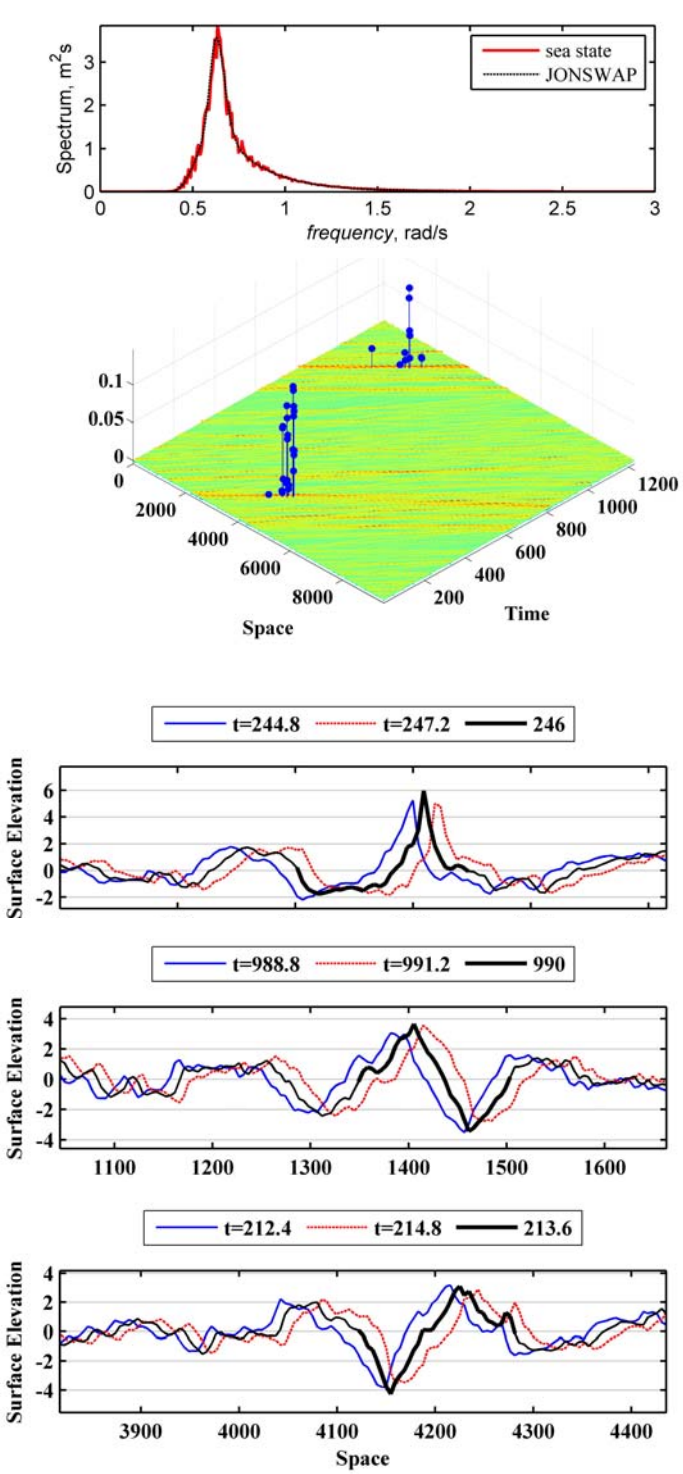

Fig. 1. Strongly numerical simulations of irregular wave trains: the initial condition (a), selection of rogue waves in space-time data sheets (b) and examples of simulated rogue waves.

Direct numerical simulations of intense irregular waves are performed for conditions of laboratory experiments and for given sea states characterized by certain spectra with the purpose to obtain the true statistics of rogue waves taking into account strongly nonlinear effects. Different problem statements are concerned: simplified narrow spectra and the JONSWAP spectrum; from weakly to fully nonlinear models; effects of occasional wave breaking on extreme wave statistics are estimated on the basis of laboratory measurements as well.

The process of irregular wave evolution is shown to be essentially non-stationary, when the Benjamin – Feir Index is large, what violates the common assumptions of statistical and kinematic theories. The transition stage is accompanied by high probability of rogue wave occurrence. Existence of long-living nonlinear wave groups (analogues of envelope solitons or breathers) is revealed in such processes due to correlations in the Fourier spectrum. Weakly nonlinear wave models are shown to be capable of reasonable statistical description of stationary conditions. Improved wave models exhibit good agreement with laboratory data.

Strongly nonlinear simulations of the primitive equations of potential hydrodynamics are used to obtain the statistical information on generation and evolution of rogue events. This data is used to shed the light onto the rogue wave occurrence: details of its appearance, evolution, and kinematics. Each realization of the given sea state, when simulated results in 10 km □ 20 min sheet of data with good resolution in time and space of the surface elevation, fluid velocity, etc. The analysis of characteristics of individual rogue waves, found in our simulations, shows the variety of their shapes and appearances. Most of the simulated rogue waves have very high crests and shallow long troughs, or sign-variable shapes. “Holes in the sea”, characterized by deep troughs, are found in the simulation data as well. In severe conditions the predominance of rogue waves with extreme rear slopes is discovered compared to rogue waves with high fronts (see Fig. 2). This kind of extreme wave asymmetry has not been mentioned in the literature before.

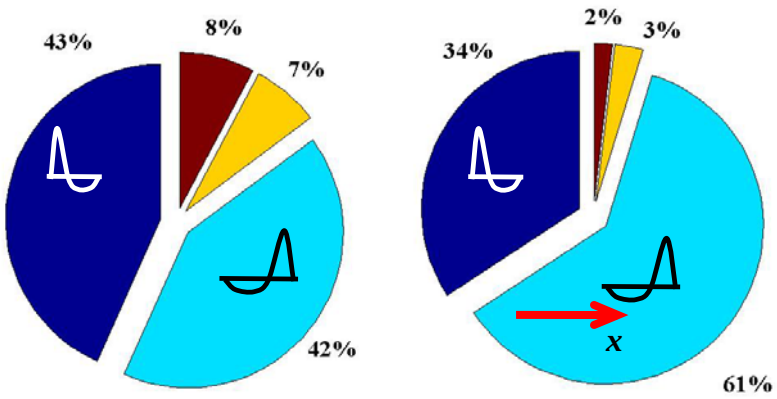

Fig. 2. Typical shapes of rogue waves in condition of moderate nonlinearity (kA_s = 0.07, left) and in severe situation (kA_s = 0.13, right).

The employed approach allows observing a full picture of the rogue wave propagation. Some of extreme waves appear suddenly and live for a short time, less then a wave period. Large amount of rogue waves’ heights oscillate with time and exceed the formal criterion of a rogue wave, $H > 2H_s$, repeatedly, and thus may be considered as *rogue events* which can live significantly longer than the wave, which satisfies the rogue wave amplitude criterion continuously (see Fig. 1). As a result, the life-time of extremely high wave events varies from several seconds to tens of characteristic wave periods.

Reconstruction of in-situ events of rogue waves

A. Slunyaev, A. Sergeeva, E. Pelinovsky, T. Talipova

In-situ measurements of oceanic rogue waves contain unique information, which is to be examined with maximal diligence. This information is always incomplete (the vast part of it are time series of the surface elevation retrieved at one location). Some in-situ registrations of rogue events may be reliably reproduced in numerical simulations when reasonable assumptions are involved. Different frameworks associated with the relation between the surface elevation and the fluid velocity fields are considered, and different numerical models are used to simulate the wave dynamics in time and space. The

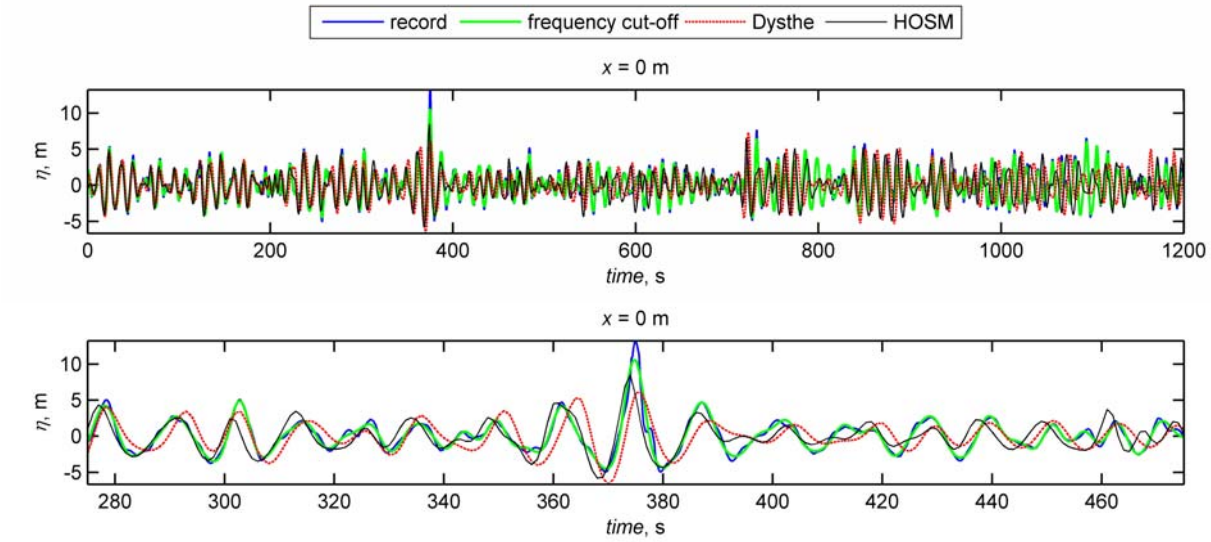

Fig. 3. The 20-min time series NA199711200151 and the extract of the rogue wave: measured and reconstructed.

reproduction of the space-time evolution of the measured waves is conducted within the frameworks of approximate equations for wave modulations, which describe the wave evolution in space. The constant-depth problem for conditions of the North Sea (North Alwyn platform) and the variable-depth conditions in Taiwanese waters (measurements from different buoys around the island) have been considered. Beyond this, the results of reconstruction are validated with help of strongly nonlinear simulations of the primitive water equations (which describe the evolution in time). The waves are very steep, what complicates the task greatly. However, sometimes the result of the reproduction procedure turns out to be rather robust, and thus provides additional information on rogue wave phenomenon. The reconstructed rogue wave is generally less steep than the measured one.

Simulations of long-living coherent wave patterns as prototypes of rogue waves

A. Slunyaev, E. Pelinovsky, A. Sergeeva

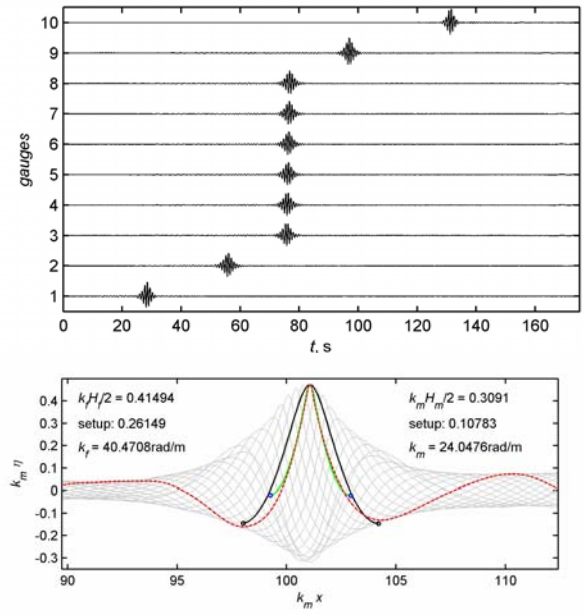

Fig. 4. Laboratory simulation of a steep envelope soliton (a), and the universal shape of maximal waves and wave envelopes caused by the modulational instability, observed in numerical simulations (c).

It has been shown already in numerous computer and laboratory simulations, and also within theoretical frameworks that irregular sea waves exhibit higher probability of extreme waves, when nonlinearity is taken into account due to phase-locked bound components and long-living nonlinear wave patterns. These nonlinear groups may be described by soliton- and breather-like analytic solutions of the approximate nonlinear Schrodinger equation (NLS). The adequacy of the NLS theory and the applicability of these solutions to extreme sea conditions of steep waves and short wave patterns have been unclear so far. We have conducted a series of works in numerical and laboratory simulations of steep waves groups with the purpose to clarify this issue.

First of all, intense envelope solitons were examined. Wave groups with steepness up to $A_{cr}\,\omega_m^2/g \approx 0.30$ are reproduced in laboratory experiments (A_{cr} is the wave crest amplitude, ω_m is the mean angular frequency and g is the gravity acceleration) (Fig. 4a). We show that the groups remain stable and exhibit neither noticeable radiation nor structural transformation for more than 60 wave lengths or about 15-30 group lengths. These solitary wave patterns differ from the conventional envelope solitons, as only a few individual waves are contained in the group. Very good agreement is obtained between the laboratory results and numerical simulations of the potential Euler equations.

We have examined the problem of the highest wave in a modulated wave train by numerical simulations of exact Euler equations. The simulations are performed for wide range of parameters. The maximal wave group has general characteristics in all cases (Fig. 4b). It is shown that in the non-breaking regimes wave crests may be amplified more than 4 times.

Some rational breather solutions of the nonlinear Schrodinger equation have been reproduced in numerical simulations within different frameworks. The simulations are validated against laboratory measurements. The focus is made to effects of strongly nonlinear wave dynamics, which cannot be considered in laboratory conditions due to technical restrictions.

Rogue wave generation on opposing jet currents due to nonlinear self-modulation

V. Shrira, A. Slunyaev

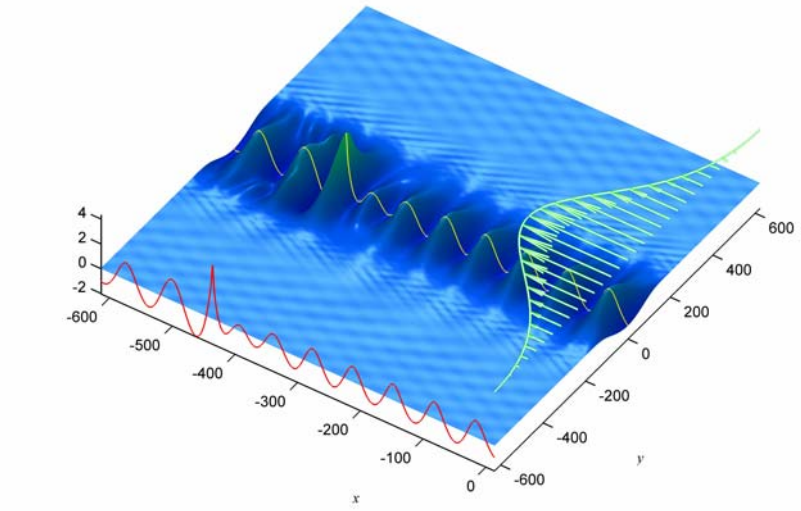

Fig. 5. Numerical simulation of a rogue wave in the field of waves trapped by a jet current

The asymptotic modal approach is developed for waves trapped by an opposing jet current in linear and nonlinear settings. Evolution equations governing dynamics of an arbitrary number of wave packets due to four-wave resonances have been derived. In particular, for a single mode the asymptotic procedure yields the integrable one-dimensional nonlinear Schrodinger equation (NLS). The NLS describes the evolution of modes along the current, while the modal structure is specified by the corresponding boundary value problem (BVP). When the current is weak in comparison with the wave celerity, the BVP reduces to the classic stationary Schrodinger equation with conditions of decay outside the jet, which allows exact solutions for a number of model current profiles. This enables us to find analytically the interaction coefficients in the dynamic equations. Thus, to the leading order a variety of analytic solutions to the evolution equation and the BVP specifying the trapped modes is readily available.

A few such asymptotic solutions are tested in numerical simulations of the Euler equations. The equations are solved by means of the adapted High Order Spectral Method. Single trapped mode solutions are simulated: the uniform waves train, modulated wave train, and solitary wave packets. The weakly nonlinear theory is shown to be a reasonable first approximation to the solution even in the case of rather steep waves. Solitary patterns of trapped waves were found to be robust, though an insignificant radiation is observed in the course of their propagation, which suggests that the solitary wave patterns represent important elements of nonlinear dynamics of gravity waves on jet currents. Their presence in the stochastic wave field may result in significant deviation from the Gaussianity, and increase the extreme wave probability.

Spectral model of nonlinear internal waves in the coastal ocean

V.V. Novotryasov, D.V. Stepanov

A spectral model of nonlinear internal gravity waves is developed. The basic component of this model is the modified Korteweg - de Vris wave equation. Using the model we studied such problem as: (I) nonlinear transformation of a tidal internal wave influenced by quadratic and cubic nonlinearity of the coastal ocean; (II) interaction between the high frequency stochastic internal waves and nonlinear tidal internal wave; (III) transformation of the stochastic internal waves influenced by quadratic nonlinearity of the coastal ocean. Features of the nonlinear transformation of the internal waves observed in various regions of the coastal ocean we compare with the model results. The model is based on the equation

$$\partial U/\partial t + c\,\partial U/\partial x - (\beta U + \beta_1 U^2)\partial U/\partial x = 0$$

$$U(t, x=0) = U_0(t),$$

The dependence of the harmonic energy of nonlinear internal waves on the harmonic number n for the distance X_{br}

$$\frac{\partial U}{\partial X} + \beta U \frac{\partial U}{\partial \tau} = 0,$$

$$U(X=0,\tau) = u_0 \sin(\omega_0 t),$$

$$U(x,t) = \sum_n^{\infty} B_n(x)\sin(n\,\omega_0 t),$$

$$B_n(x) = \frac{2u_0}{(nx/X_{br})} J_n(nx/X_{br}),$$

$$X_{br} \sim \beta^{-1}\frac{c^2}{(u_0\omega_0)},$$

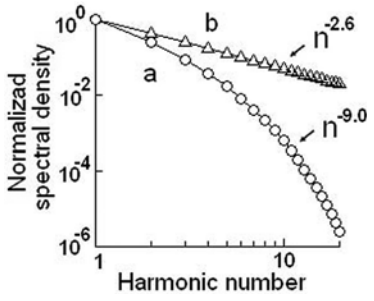

Fig. 1. The dependence of the normalized harmonic energy of nonlinear internal waves on the harmonic number n for the two distances: $r_1 \sim 0.5\ X_{br}$ (line a) and $r_2 \sim X_{br}$ (line b), where X_{br} is the distance between the areas of generation and internal wave breaking.

Nonlinear Internal Gravity Wave Model Spectra

Let the intertail gravity waves at the boundary x=0 is superposition waves with tidal frequency Ω and random high-frequency internal wave with a typical frequency $\omega_* \gg \Omega$ and the dispersion $\sigma^2 = <\xi_0^2>$

$$\eta_0(t) = A\cos(\Omega t + \psi) + \xi_0(t),$$

$$Sp_\eta(\omega, x) = \sum_{n=-\infty}^{\infty} \frac{J_n^2(A\bar{\beta}n)\exp\{-(\sigma\bar{\beta}n)^2\}}{(\bar{\beta}n)^2} \times \delta(\omega_n) +$$

$$+ \sum_{n=-\infty}^{\infty} \frac{J_n^2(\bar{\beta}A)}{2\pi\bar{\beta}^2}\exp\{-(\bar{\beta}\sigma)^2\}\delta(\omega_n)\times,$$

$$\times \int_{-\infty}^{+\infty} [\exp\{B_0(s)(\bar{\beta}x)^2\} - 1]\exp[i(\omega_n)s]ds \qquad (2)$$

where $\omega_n = \omega - n\Omega$, $\bar{\beta} = \beta x\Omega$, $\bar{\beta} = \beta x\Omega$

The second series in the (2) is the spectrum of the liner random waves distorted by interaction with tide. Define the frequency band of the random waves as $\omega \in [\omega_l' = \omega_h/(1+d_T), \omega_h' = \omega_h/(1-d_T)]$. The spectrum of waves we can write in the following form

$$\underline{\underline{Sp_{\xi}(\omega, x) \simeq \frac{\sigma^2}{\omega\pi\beta x A\Omega} \equiv K \cdot \omega^{-1}}}$$

Let us consider transformation of the intensity spectrum of the vertical displacements of the inertial gravity waves. We assume that the wave field $\eta(t,0) = \eta(t)$ at the boundary $x = 0$ is statistically homogeneous and is described by the covariant function $B_0(\tau) = \sigma_0^2 R(\tau)$, where $\sigma_0^2 = B(0) = \overline{\eta}_0^2$ and R is the correlation coefficient.

The spectrum of the vertical displacements is the:

$$Sp_{\eta}(\omega; x) = (2\pi\beta\omega x)^{-2} \exp[-(\sigma_0\beta\omega x)^2] \times$$
$$\times \int_{-\infty}^{\infty} \{\exp[B_0(\tau)(\beta\omega x)^2] - 1\} \exp(i\omega\tau) \cdot d\tau .$$

Let us consider the spectra $\omega \to \infty$. In this case,

$$Sp_{\eta}(\omega; x) \sim \omega^{-3}(\beta x)^{-3}\sqrt{2\pi/\nu}\exp[-(\sigma_0\beta\omega x)^2/2] .$$

It follows from the obtained expression that the spectrum of nonlinear inertial gravity waves for $\sigma_0\beta x << 1$ with $\omega \to \infty$ decreases according to a power law

$$\underline{\underline{Sp_{\eta}(\omega; x) \sim \omega^{-3}}} .$$

The Model Spectrum of Internal Tidal Waves influenced by the cubic nonlinearity

$$\frac{\partial U}{\partial X} + (\alpha U + \alpha_1 U^2)\frac{\partial U}{\partial \tau} = 0 ,$$
$$U(X = 0, t) = u_0 \sin(\omega_0 t) ,$$
$$Sp(\omega, X) = \frac{1}{2\pi}\int_{-\infty}^{+\infty} U(\tau, X)\, e^{-i\omega\tau} d\tau$$

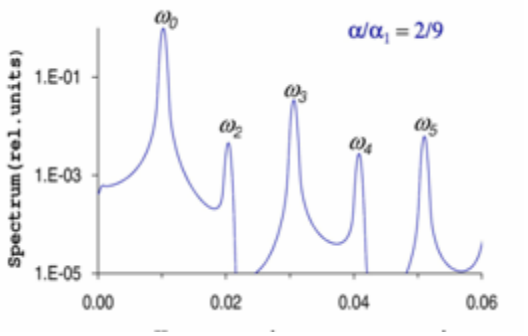

Fig. 2. The normalized model spectrum of horizontal kinetic energy of nonlinear internal tide in the area of breaking influenced by the cubic nonlinearity.

Spectra of Nonlinear Internal Waves in the coastal ocean

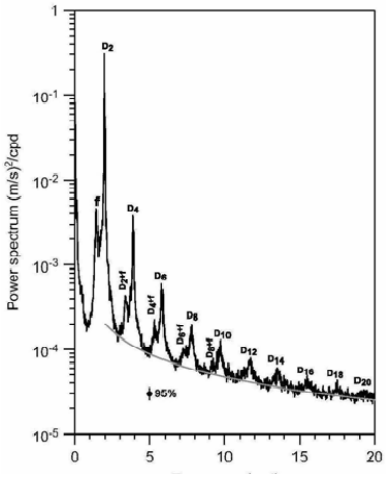

Bay of Biscay (*Deep Sea Res.* 2007. V. 54. P. 533)

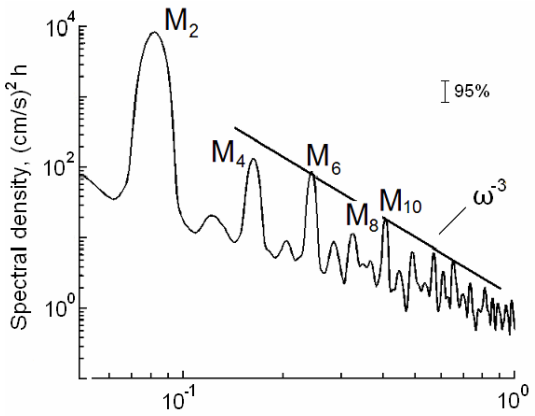

Gulf of California (*Geophys. Res. Letters*, , 2011. V. 38, L24611, doi:10.1029/2011GL049886)

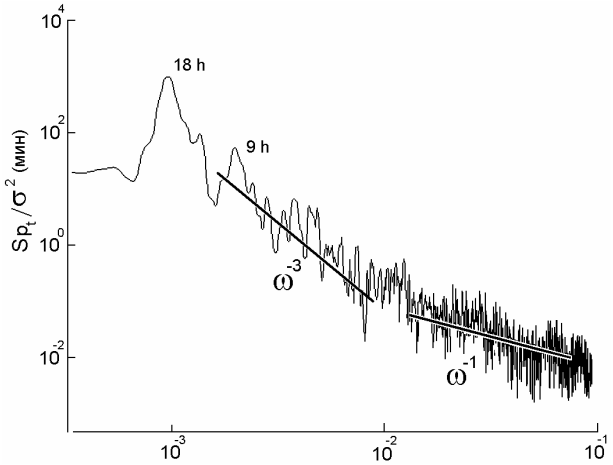

Peter the Great Bay (*Nonlin. Processes in Geophys.*, 2007, V.14, P. 757)

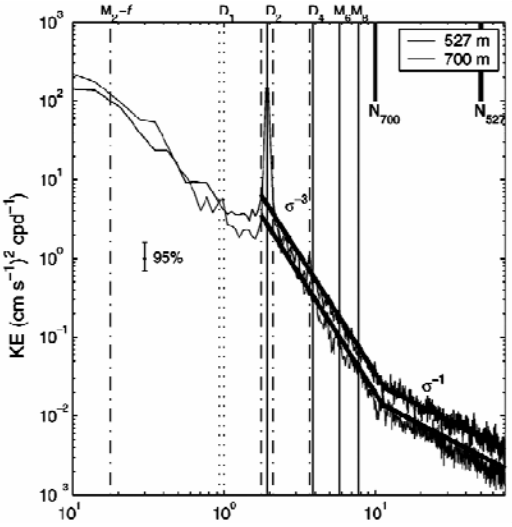

Shelf of England (*Deep Sea Res*. 2006. V. 53. P. 627)

Fig. 3 Spectra of Nonlinear Internal Waves in the coastal ocean

Effects of internal waves in a shoaling thermocline

V. Navrotsky

As a result of complex experiments and observations in the Japanese Sea shelf zone it was shown that internal waves in a shoaling thermocline do not break at once, but transform into discreet series of stratified volumes of cold water (boluses). These boluses propagate to shores rather far from the zone of thermocline-bottom contact, i.e. into a zone of non-stratified waters. The process is analogous to the uprush of surface waves on a beach. While moving to shallower waters, internal waves and boluses are destroying gradually: a) beginning from the close-to-bottom parts in the case of the strong thermocline and long-period waves (Fig. 1); b) simultaneously in the top and bottom parts for short-period waves (Fig.2).

Destruction of internal waves and boluses in shallowing thermocline leads to: a) sharp increase in horizontal and vertical velocities in the close-to-bottom layers (Fig.3); 2) generation of three-dimensional and quasi-horizontal turbulence, and consequently, to horizontal and vertical momentum fluxes of the same order of magnitude as in the upper mixed layer (Fig. 4). These processes are extremely important for nutrient and turbidity fluxes, as well as for bottom morphology in shelf zones of sea.

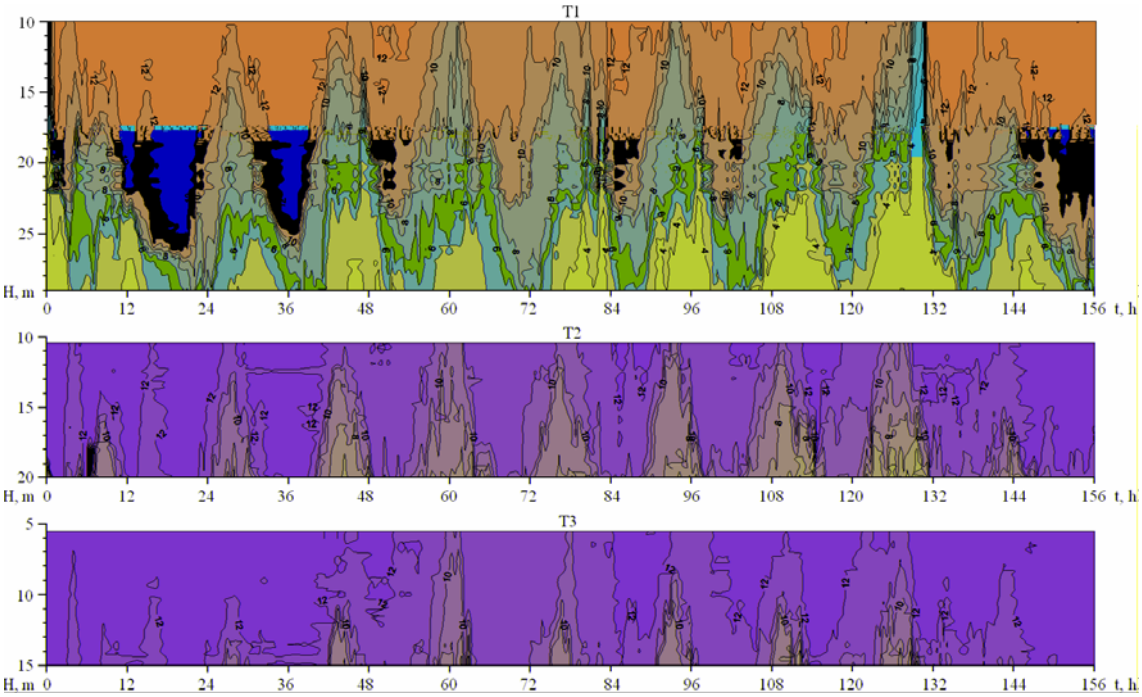

Fig. 1. Temporal sections of temperature field showing internal waves and their transformation into discreet series of boluses in near-bottom layers with different bottom depth.

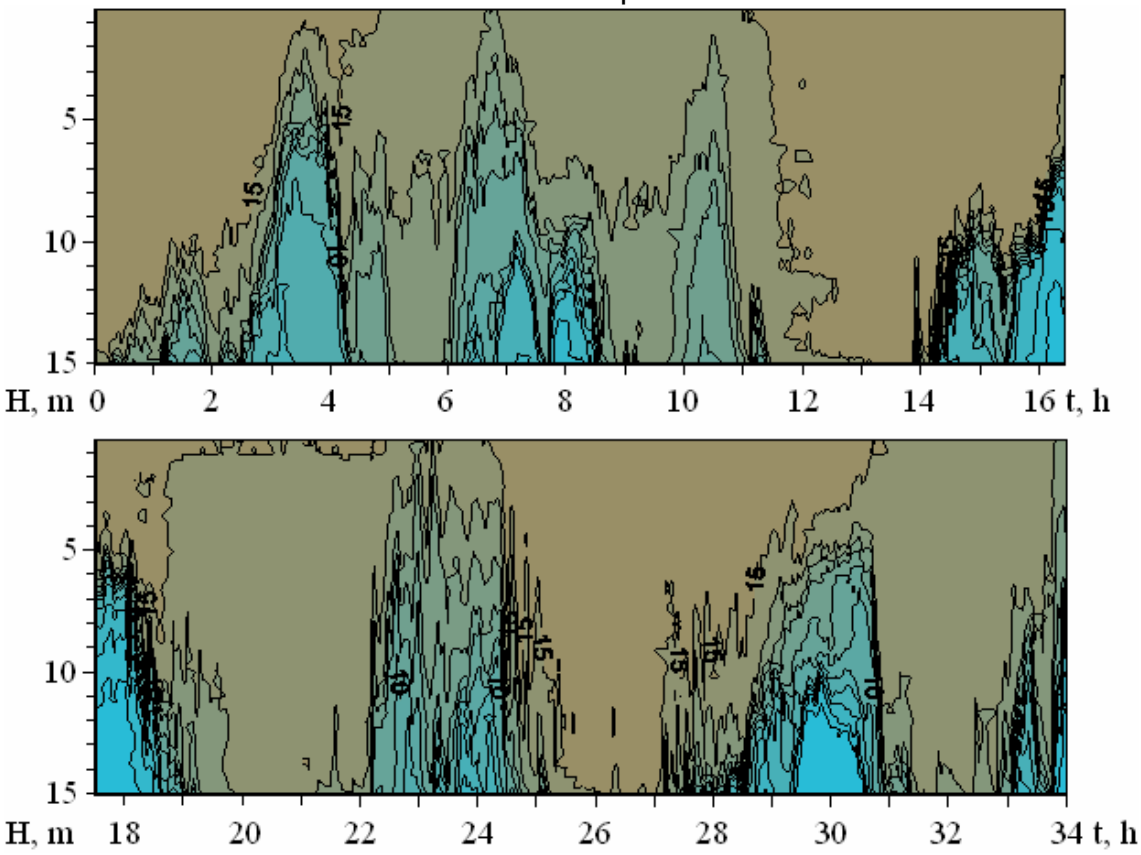

Fig.2. Destroying of boluses generated by short-period internal waves in the near-bottom thermocline.

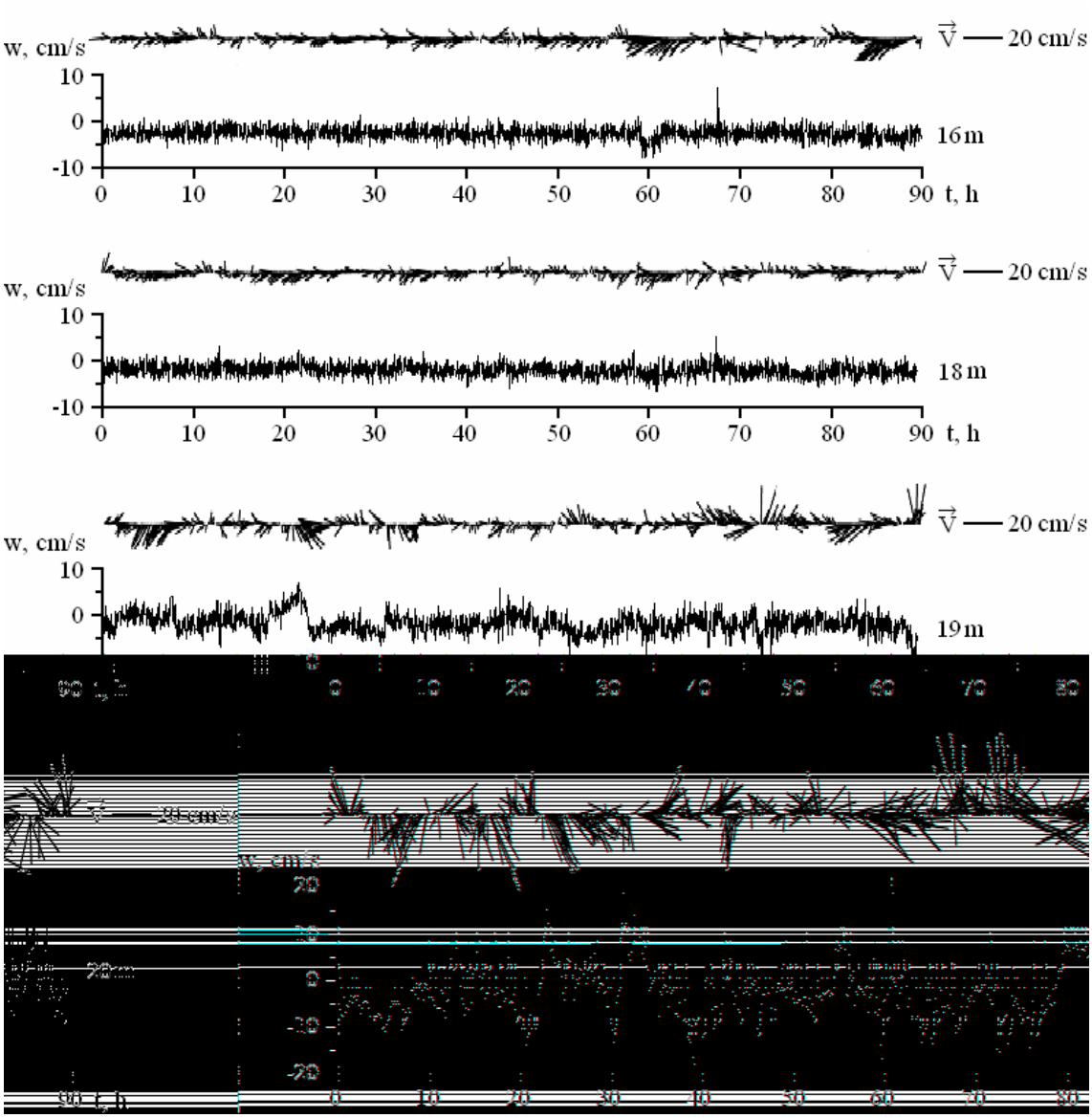

Fig. 3. Vectors of horizontal current velocities and vertical components ***w*** at different levels in a near-bottom layer with boluses. The bottom depth is 22 m.

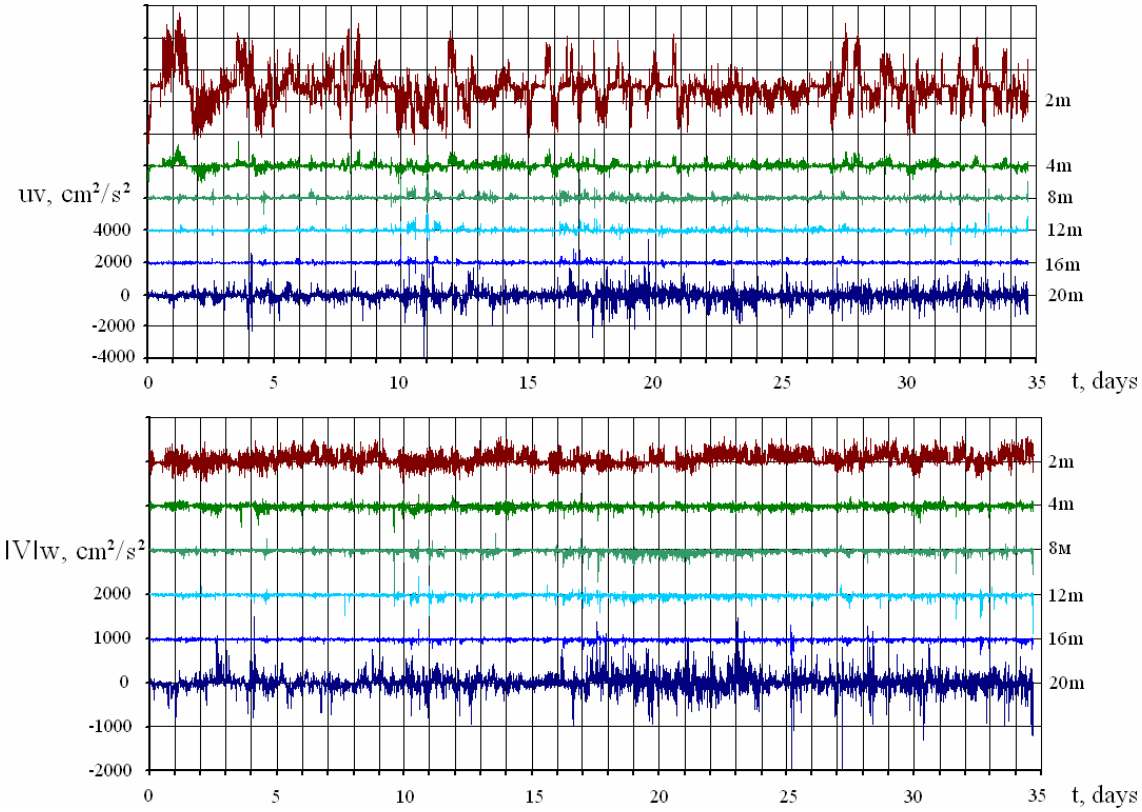

Fig. 4. Horizontal (uv) and vertical (|Vlw) momentum fluxes (with constant density approximation) at different levels. Bottom depth is 22 m.

Dissipation-derived estimates of entrainment in the Denmark Strait overflow plume

V. Paka

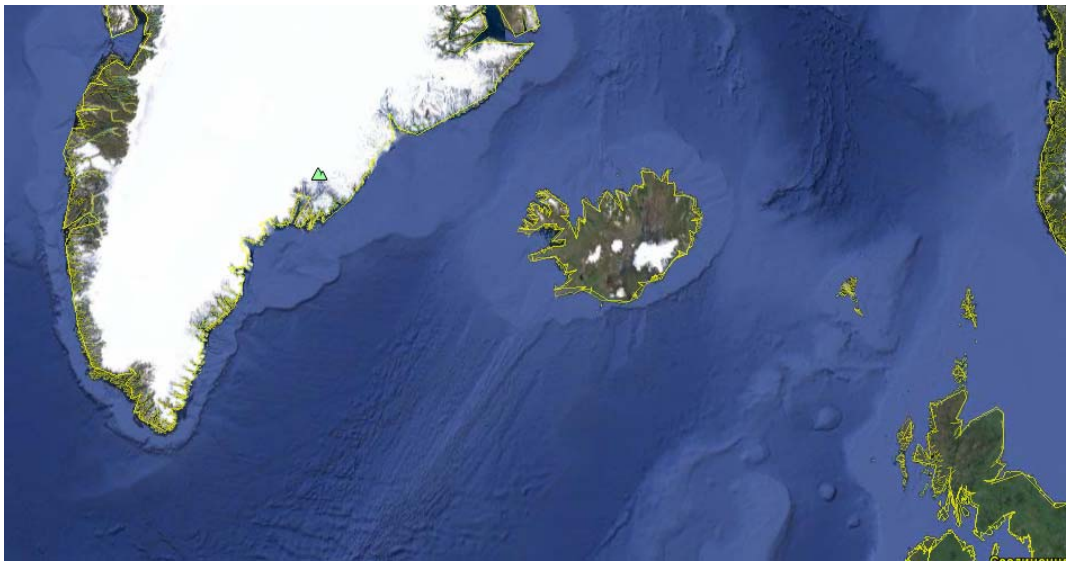

To examine processes controlling the entrainment of ambient water into the Denmark Strait overflow (DSO) plume (fig. 1), measurements of turbulent dissipation rate were carried out by a quasi free-falling (loosely tethered) microstructure sounde (MSS). The MSS was specifically designed to collect data on dissipation-scale turbulence and fine thermohaline stratification in any ocean layer to depth of 3500 m. The task was to perform microstructure measurements in the DSO plume in lower 300 m depth interval including bottom mixed layer and interfacial layer below the non-turbulent ambient water. MSS was attached to Rosette water sampler equipped with SeaBird CTDO and LADCP, the tether's end fastened to the rack, for delivery of MSS to the chosen depth where it was remotely released from the rack for performing measurements in free-falling mode.

Using the measured vertical profiles of dissipation, the entrainment rate as well as bottom and interfacial stresses were estimated in the DSO plume at a distance of 200 km downstream the sill. Dissipation-derived estimates of entrainment are much smaller than bulk estimates of entrainment calculated from the downstream change of the mean properties in the plume, suggesting the lateral stirring due to meso-scale eddies rather than diapycnal mixing to be the main contributor to entrainment. Dissipation-derived bottom stress estimates are roughly one-third the magnitude of those from log velocity profiles. In the interfacial layer, the overturning scale extracted from conventional CTD data (the Thorpe scale) was found to be proportional to the Ozmidov scale calculated from turbulence dissipation rate and buoyancy frequency, with the proportionality constant of 1.1±0.7 and the correlation of 0.77.

Observations of mode 2 internal waves on shelf of the Black Sea

A. Serebryany

Long-term measurements performed from the stationary oceanographic platform on shelf of the Black Sea (Katsiveli, in summer of 2011 and 2013) revealed existence intense internal waves of 17 h inertial periods. Observations were made by thermistor string, looking down ADCP, every hour repeated CTD soundings. Those waves caused substantial oscillations of temperature and the sound speed in the water bulk. The main feature of the observed phenomena was the existence of not only first but also the second internal wave mode (Figs. 1 and 2). Moreover, we observed short-period internal waves (with periods of several minutes) of the second mode as well. In the Black Sea, internal waves of the second mode were observed for the first time.

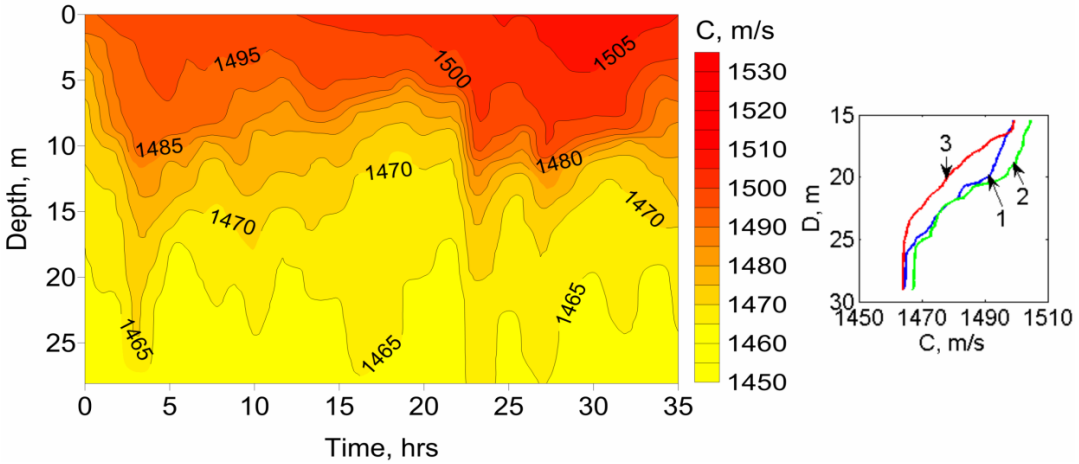

Fig. 1. Oscillations of the sound-speed isopleths under the influence of the first-mode quasi-inertial internal waves (July 11 to 12, 2011). Vertical profiles of sound speed are shown on the right for characteristic times of July 11 (1) 4.00, (2) 23.00, (3) 12.00 h).

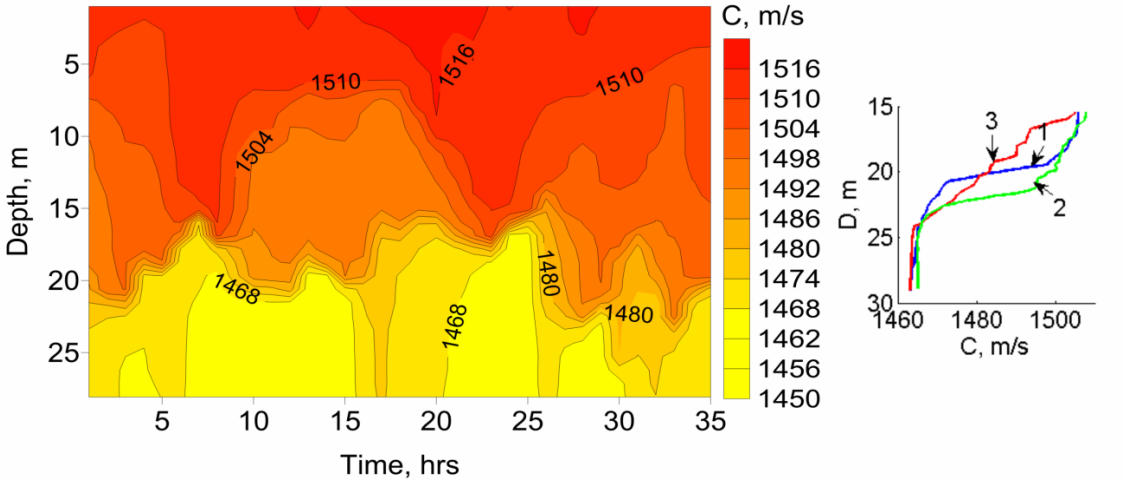

Fig. 2. Same as in Fig. 1, but for the second-mode inertial internal waves (July 17 to 18, 2001). Vertical profiles of the sound speed for characteristic times on July 17 (1) 6.00, (2) 14.00, and (3) 24.00 h).

References:

Arashkevich, E. G., A. V. Drits, A. G. Timonin, and V. V. Kremenetskiy, Variability of spatial distribution affected by the water dynamics in the northeastern part of the Black Sea, Oceanology, 42, Suppl. 1, S79– S94, 2002b.

Chabchoub, A., Hoffmann, N., Onorato, M., Slunyaev, A., Sergeeva, A., Pelinovsky, E., and Akhmediev, N. Observation of a hierarchy of up to fifth-order rogue waves in a water tank. Phys. Rev. E 86, 056601-1–6 (2012).

Dolgikh G. I., V. V. Navrotskii, and E. D. Kholodkevich. Internal Waves in the Near Bottom Thermocline and Microdeformations in the Earth's Crust in the Continent–Ocean Transition Zone. Doklady Earth Sciences, 2011, Vol. 438, Part 2, pp. 810–814.

Dubina V.A., Fayman P.A., Ponomarev V.I. Vortex structure of currents in Peter the Great Bay. Izvestiya TINRO. 2013. Vol. 173. P. 247-258 (In Russsian).

Filonov A., Novotraysov V. On a spectrum of nonlinear internal waves in the oceanic coastal zone. Nonlin. Proc. Geophys. 2007. V.14. P. 757-762

Filyushkin B.N., Sokolovskiy M.A. 2011 Modeling the evolution of intrathermocline lenses in the Atlantic Ocean. J Mar Res, 69: 191-220.

Fine, I.V., Kulikov, E.A., and Cherniawsky, J.Y. (2013), Japan's 2011 tsunami: Characteristics of wave propagation from observations and numerical modeling, Pure Appl. Geophys., 170, 1295-1307; doi 10.1007/s00024-012-0555-8.

Gulev S, Belyaev K., Probability distribution characteristics for surface air–sea turbulent heat fluxes over the Global Ocean. J. Climate, 25 (2012), 1,184-206

Gulev S., K. Belyaev, Probability distribution characteristics for surface air-ocean turbulent heat fluxes over World Ocean. J. Climate, 184-206, 2012

Ivanov V.A., Belokopytov V.N., 2013 Oceanography of the Black Sea. National Academy of Sciences of Ukraine, Marine Hydrophysical Institute, Sevastopol, 210 p.; ECOSY-Gidrofizika., ISBN: 978-966-022-6165-5

Khartiev S.M., Morozov E.G., Grigorenko K.S., Matishov D.G., Solov'ev A.N., and Solov'eva A.A., Internal waves in a stratified sea with layers of density inversions, Doklady Earth Sciences, 2013, Vol. 448, Part 1, pp. 70–73.

Kleshcheva T.I., Permyakov M.S. The influence of spatial variability of sea surface temperature on wind field // Current problems in remote sensing of the Earth from Space. –2012. –Vol.9, №3. –C.216-223 (in Russian).

Knysh, V. V., Korotaev, G. K., Moiseenko, V. A., Kubryakov, A. I., Belokopytov, V. N., and Inyushina, N. V.: Seasonal and interannual variability of Black Sea hydrophysical fields reconstructed from 1971–1993 reanalysis data // Izv. Atmos. Ocean. Phyhs., 47, 399–411, 2011.

Konstantinov O. and Novotryasov V. Surface manifestations of internal waves observed using a land based video system. Izv., Atm. and Oceanic Phys. 2013. V. 49. P. 334–338.

Korotaev G.K. (1997), Circulation in semi-enclosed seas induced by buoyancy flux through strait. In: Sensitivity to change: Black Sea, Baltic Sea and Northern Sea, Eds. E. Ozsoy, A. Mikaelyan. NATO ASI Ser. 2, Vol.27, Dordrecht,The Netherlands, Kluwer Acad. Publ., 1997, 197-210.

Korotaev G., Oguz T., Nikiforov A., and C. Koblinsky (2003), Seasonal, interannual, and mesoscale variability of the Black Sea upper layer circulation derived from altimeter data. J. Geophys. Res., 108 (C4), 3122,doi:10.1029/2002JC001508.

Kubryakov A.A. Stanichny S.V. Mean dynamic topography of the Black Sea, computed from altimetry, drifters measurements and hydrology data // Ocean Science.– 2011. № 7.– P. 745-753.

Kubryakov A. A. and Stanichny S. V. Estimating the Quality of the Retrieval of the Surface Geostrophic Circulation of the Black Sea by Satellite Altimetry Data Based on Validation with Drifting Buoy Measurements // Izv. Atmos. Ocean. Phyhs., 2013, Vol. 49, No. 9, pp. 930–938.

Kukarin V.F., Lyapidevsky V.Yu., Navrotsky V.V., Khrapchenkov F.F. Evolution of internal waves of large amplitude in the shelf zone of sea. Fundamental and applied hydrophysics. 2013. Vol. 6. No. 2. P. 35-45. (In Russian)

Marchenko A.V. Morozov E.G., Muzylev S.V., A Tsunami Wave Recorded near a Glacier Front, Natural Hazards and Earth System Sciences, Vol. 12, 2012, pp 415-419.

Marchenko A, Morozov E, Muzylev S., Measurements of sea-ice flexural stiffness by pressure characteristics of flexural-gravity waves, Annals of Glaciology 54(64), pp. 1-10, 2013

Marchenko A.V., E.G. Morozov, Asymmetric tide in Lake Vallunden (Spitsbergen), Nonlinear Processes Geophys., Vol. 20, p. 935–944, 2013.

Mercier H., P. Lherminier, A. Sarafanov, F. Gaillard, N. Daniault, D. Desbruyeres, A. Falina, B. Ferron, C. Gourcuff, T. Huck, V. Thierry (2014), Variability of the meridional overturning circulation at the Greenland–Portugal Ovide section from 1993 to 2010, Progress in Oceanography, Vol. 129, doi:10.1016/j.pocean.2013.11.001.

Morozov E.G., Marchenko A.V., Short-period internal waves in an Arctic fjord (Spitsbergen), Izv. Atmosph. Oceanic Physics, Vol. 48, 2012, No. 4, pp. 401–408.

Morozov E.G., Tarakanov R.Yu., Discovery Gap: the terminal point of Antarctic Bottom Water spreading, Doklady Earth Sciences, Vol. 446, No. 2, pp. 1190–1192, 2012.

Morozov E.G., Tarakanov R.Yu., Zenk W., Spreading of Antarctic Bottom Water in the Atlantic Ocean, Geography, Environment, Sustainability Vol. 4., № 5, 2012, 24-32.

Morozov E.G., Strong flows of bottom water in abyssal channels of the Atlantic, Without Bounds: A Scientific Canvas of Nonlinearity and Complex Dynamics, Springer, 707-718, 2013.

Morozov E. G. and R. Yu. Tarakanov, The Flow of Antarctic Bottom Water from the Vema Channel to the Brazil Basin, Doklady Earth Sciences, 2014, Vol. 456, Part 1, pp. 598-601.

Morozov E. G., R. Yu. Tarakanov, and H. van Haren, Transport of AABW through the Kane Gap, tropical NE Atlantic Ocean, Ocean Sciences, Vol. 9, 825-835, 2013. doi 10.5194/os-9-825-2013

Morozov E. G., R.Yu. Tarakanov, I. Ansorge, S. Swart, Jets and Transport of the Antarctic Circumpolar Current in the Drake Passage, Fundamental and Applied Hydrophysics, V. 7, №3, 23-28, 2014.

Morozov E.G., A.V. Marchenko, Yu.V. Fomin, Supercooled Water near the Glacier Front in Spitsbergen, Izvestia RAN, ser. Fizika Atmosfery i Okeana, Vol. 51, No. 2, pp. 203–207, 2015.

Morozov E.G., Strong Flows of Bottom Water in Abyssal Channels of the Atlantic, Week of Science, Springer, 2013.

Murdmaa I. O., Borisov D. G., Demidova T. A., Ivanova E. V., Levchenko O. V., Marinova Y. G., Mutovkin A. D., Putans V. A., Humbs P., Skolotnev S. G., Peyve A. A. Very high resolution seismic profiling at the Brazil Margin, EOS, Trans. AGU, v. 93(25), p. 233, 2012. doi:10.1029/2012EO250002

Navrotsky V.V., Lyapidevsky V.Yu., Pavlova T.P., Khrapchenkov F.F. Internal waves and mixing in the shelf zone. Izv. TINRO. 2010. Vo. 162. P. 324-337. (In Russian, with English abstract)

Navrotsky V.V., V.Yu. Lyapidevsky, E.P.Pavlova. Internal waves and their biological effects in the shelf zone of sea. Vestnik FEB RAS. 2012. No.6. P. 22-31. (In Russian)

Navrotsky V.V., Liapidevskii V.Yu., E.P.Pavlova. Features of internal waves in a shoaling thermocline. International Journal of Geosciences. 2013. Vol. 4. No. 5. P.871-879.

Novotryasov V. and Yaroshchuk I. On the propagation of long nonlinear internal waves against the background of statistical inhomogeneities of density field. Izv., Atm. and Oceanic Phys. 2011. V. 47. P. 649–652.

Novotryasov V., Filonov A. and Lavín M. Nonlinear internal tidal waves in a semi-enclosed sea (Gulf of California). Geophys. Res. Lett. 2011. V. 38. L24611.

Novotryasov V., Pavlova E. Determination of parameters of low-frequency internal waves in the coastal zone of a fringing sea using field measurements and basing on the nonlinear theory. Rus. Met. Hydr. 2011. V. 36. P. 269-272,

Paka, V. T., B. Rudels, D. Quadfasel, and V. M. Zhurbas (2010), Measurements of Turbulence in the Zone of Strong Bottom Currents in the Strait of Denmark, Doklady Earth Sciences, 432(1), 613–617.

Paka V., V. Zhurbas, B. Rudels, D. Quadfasel, A. Korzh, and D. Delisi. Microstructure measurements and estimates of entrainment in the Denmark Strait overflow plume. Ocean Sci., 9, 1–12, 2013 www.ocean-sci.net/9/1/2013/ doi:10.5194/os-9-1-2013

Pakhomova S, E. Vinogradova, E. Yakushev, A. Zatsepin, G. Shtereva, V. Chasovnikov, O. Podymov. Interannual variability of the Black Sea Proper oxygen and nutrients regime: rregime: The role of climatic and anthropogenic forcing // Journal of Estuarine, Coastal and Shelf Science, 140 (2014) 134 -145.

Permyakov M.S., Tarkhova T.I. The wind and sea surface temperature anomalies over the Kashevarov Bank in Okhotsk Sea// Current problems in remote sensing of the Earth from Space. –2011. –Vol.8, №3. –C.277-282 (in Russian).

Piotukh V.B., Zatsepin A.G., Kazmin A.S., Yakubenko V.G. Impact of winter cooling on the variability of thermohaline characteristics of active layer in the Black Sea, Oceanology. 2011. V.51. No.2. P. 222-230.

Ponomarev V.I., Fayman P.A., Mashkina I.V., Dubina V.A. Simulation of mesoscale circulation in the northwestern Japan Sea. Morskoi Gidrofizicheskii Zurnal, MGI, Sevastopol, 2013b, 5, P. 51-63 (In Russsian).

Ponomarev V., Petrova V.A., Dmitrieva E. Climatic variability of the surface heat fluxes in the North Pacific. Izvestiya TINRO. 2012. Vol. 169. P. 67-76. (in Russian).

Ponomarev V., Dmitrieva E., Shkorba S., Savelieva N.I. Inter-related climate anomalies in the Pacific Ocean and Far Eastern Seas. P.13-36. In: Oceanographic studies of the Far Eastern Seas and North-Western Pacific. Editor V.A. Akulichev. Vladivostok, Dalnauka, 2013 (in Russian).

Prants, S., Budyansky, M., Ponomarev, V., Uleysky, M., 2011. Lagrangian study of transport and mixing in a mesoscale eddy street. Ocean Modeling. 38, P. 114–125.

Prants, S.V., Ponomarev, V.I., Budyansky, M.V., Uleysky, M.Y., Fayman, P.A., 2013. Lagrangian analysis of mixing and transport of water masses in the marine bays. Izvestiya Atmos. Oceanic Phys. 49. P. 82–96.

Prants, S.V., Ponomarev, V.I., Budyansky, M.V., Uleysky, M.Y., Fayman, P.A. Lagrangian analysis of vertical structure of eddies simulated in the Japan Basin of the Japan / East Sea. Ocean Modeling. 2015. 86. P.128-140.

Rabinovich, A.B., Candella, R.N., and Thomson, R.E. (2013), The open ocean energy decay of three recent trans-Pacific tsunamis, Geophys. Res. Lett., 40, doi:10.1002/grl.50625.

Sarafanov A., A. Falina, H. Mercier, A. Sokov, P. Lherminier, C. Gourcuff, S. Gladyshev, F. Gaillard, and N. Daniault (2012), Mean full-depth summer circulation and transports at the northern periphery of the Atlantic Ocean in the 2000s, Journal of Geophysical Research, 117, C01014, doi:10.1029/2011JC007572.

Serebryany A., I. Khymchenko. Strong variability of sound speed field on shelf of the Black Sea caused by internal inertial waves. Proceedings of Forum Acusticum. 7-12 September, 2014, Krakow, Poland.

Sergeeva, A., Slunyaev, A., Pelinovsky, E., Talipova, T., and Doong, D.-J. Numerical modeling of rogue waves in coastal waters. Nat. Hazards Earth Syst. Sci. 14, 861–870 (2014). doi:10.5194/nhess-14-861-2014

Sergeeva, A., Slunyaev, A. Rogue waves, rogue events and extreme wave kinematics in spatio-temporal fields of simulated sea states. Nat. Hazards Earth Syst. Sci. 13, 1759-1771 (2013). doi:10.5194/nhess-13-1759-2013

Shrira, V.I., Slunyaev, A.V. Trapped waves on jet currents: asymptotic modal approach. J. Fluid Mech. 738, 65-104 (2014).

Shrira, V.I., Slunyaev, A.V. Nonlinear dynamics of trapped waves on jet currents and rogue waves. Phys. Rev. E. 89, 041002(R) 1–5 (2014).

Shkorba S.P., Ponomarev V.I., Dmitrieva E.V., Kuimova L.N. Long wave of interdecadal oscillation in moderate latitudes of the Asian Pacific. 2nd Int. Symposium on Effect of Climate Change on the World's Oceans, Yeosu, Korea, May 13-20, 2012. http://pices.int/publications/presentations/2012-Climate-Change/S1/Day2-1215-Shkorba-S1.pdf).

Slunyaev, A., Didenkulova, I., and Pelinovsky, E. Rogue waters. Contemporary Physics. 2011, vol. 52, No. 6, 571 – 590.

Slunyaev, A.V. and Sergeeva, A.V. Stochastic simulation of unidirectional intense waves in deep water applied to rogue waves JETP Letters, 2011, Vol. 94, No. 10, pp. 779–786.

Slunyaev, A., Pelinovsky, E., Guedes Soares, C. Reconstruction of extreme events through numerical simulations. Journal of Offshore Mechanics and Arctic Engineering. 136(1), 011302 (2014). doi:10.1115/1.4025545

Slunyaev, A., Clauss, G.F., Klein, M., Onorato, M. Simulations and experiments of short intense envelope solitons of surface water waves. Phys. Fluids 25, 067105,1-17 (2013).

Slunyaev, A., Pelinovsky, E., Sergeeva, A., Chabchoub, A., Hoffmann, N., Onorato, M., Akhmediev, N. Super rogue waves in simulations based on weakly nonlinear and fully nonlinear hydrodynamic equations. Phys. Rev. E 88, 012909–1-10 (2013).

Slunyaev, A.V., Shrira, V.I. On the highest non-breaking wave in a group: fully nonlinear water wave breathers vs weakly nonlinear theory. J. Fluid Mech. 735, 203-248 (2013).

Sokolovskiy M.A., Filyushkin B.N., Carton X.J. Dynamics of intrathermocline vortices in a gyre flow over a seamount chain. Ocean Dynamics, 2013, v. 63, N 7, pp. 741-760.

Stepanov D. and Novotryasov V. Internal Kelvin wave frontogenesis on the equatorial pycnocline // Geophys. Astrophys. Fluid Dyn. 2011. V. 105. P. 438 - 452.

Stepanov D. and Novotryasov V. Sub-inertial modulation of nonlinear Kelvin waves in the coastal zone. Nonlin. Proc. Geophys. 2013. V. 20. P. 357–364.

Tarakanov R. Yu., E. G. Morozov, A. M. Gritsenko, T. A. Demidova, and N. I. Makarenko, Transport of Antarctic Bottom Water through Passages in the East Azores Ridge (37° N) in the East Atlantic Oceanology, 2013, Vol. 53, No. 4, pp. 432–441.

Tarakanov R.Yu., N.I. Makarenko, E.G. Morozov, Antarctic Bottom Water Flow in the Western Part of the Romanche Fracture Zone Based on the Measurements in October of 2011, Oceanology, Vol. 53, No. 6, pp. 655–667, 2013.

Tarakanov R.Yu., E.G. Morozov, Flow of Antarctic Bottom Water at the Output of the Vema Channel, Oceanology, Vol. 55, No. 2, pp. 153–161, 2015.

Tarkhova T.I., Permyakov M. S., Potalova E. Yu., and Semykin V. I. Sea surface wind perturbations over the Kashevarov Bank of the Okhotsk Sea: a satellite study. Annales Geophysicae, 2011, Vol .29, 393-399, doi:10.5194/angeo-29-393-2011.

Trusenkova O., Kaplunenko D. 2013. Variability modes of sea level in the Sea of Japan. Oceanology, 53(3), 308–316.

Trusenkova O. Variability of eddy kinetic energy in the Sea of Japan from satellite altimetry data. Oceanology, 54(1), 8–16.

van Haren H., E. Morozov, L. Gostiaux, R. Tarakanov, Convective and shear-induced turbulence in the deep Kane Gap, J. Geophys. Res.: OCEANS, Vol. 118, p. 5924–5930, 2013, doi:10.1002/2013JC009282, 2013.

van Haren H., L. Gostiaux, E. Morozov, and R. Tarakanov, Extremely long Kelvin-Helmholtz billow trains in the Romanche Fracture Zone, Geophysical Research Letters, Vol. 41, 2014.

Yunev, O.A., V.I. Vedernikov, O. Basturk, A. Yilmaz, A. E. Kideys, S, Moncheva, and S. Konovalov, Long-term variations of surface chlorophyll-a and primary production in the open Black Sea, Mar. Ecol. Prog. Ser., 230, 11-28, 2002.

Zatsepin, A.G. A.I. Ginzburg, A.G. Kostianoy, Observations of the Black Sea mesoscale eddies and associated horizontal mixing, Journal of Geophysical Research. 2003. V.108. P. 3246–3272.

Zatsepin A.G., Denisov E.S., Emel'yanov S.V., Kremenetskiy V.V., Poyarkov S.G., Stroganov O.Yu., Stanichnaya R.R., and Stanichny S.V., 2005 Effect of Bottom Slope and Wind on the Near-Shore Current in a Rotating Stratified Fluid: Laboratory Modeling for the Black Sea / Oceanology. 2005. V. 45, Suppl. 1. P. S13-S26.

Zhurbas V., J. Elken, V. Paka, J. Piechura, G. Väli, I. Chubarenko, N. Golenko, and S. Shchuka, (2012), Structure of unsteady overflow in the Słupsk Furrow of the Baltic Sea, J. Geophys. Res. – Oceans, 117, C04027, doi:10.1029/2011JC007284

Zolina O., Simmer C., Belyaev K., Kolterman P., Gulev S., Changes in the duration of European wet and dry spells during the last decade. J. Climate, 25, (2012), 24. 25189-25198.